

Characterizing magma fragmentation and its relationship with eruptive styles of Somma-Vesuvius volcano (Naples, Italy)

Matthieu Poret ^{a,*}, Miriana Di Donato ^b, Antonio Costa ^d, Roberto Sulpizio ^c, Daniela Mele ^c, Federico Lucchi ^b

^a Université Clermont Auvergne, CNRS, IRD, OPGC, Laboratoire Magmas et Volcans, Clermont-Ferrand, France

^b Università di Bologna, Dipartimento di Scienze Biologiche, Geologiche e Ambientali, Bologna, Italy

^c Università di Bari, Dipartimento di Scienze della Terra e Geoambientali, Bari, Italy

^d Istituto Nazionale di Geofisica e Vulcanologia, Sezione di Bologna, Bologna, Italy



ARTICLE INFO

Article history:

Received 6 May 2019

Received in revised form 1 October 2019

Accepted 2 October 2019

Available online 18 November 2019

Keywords:

Total grain-size distribution

Bulk granulometry

Eruption source parameters

Tephra fallout

Volcanic hazards assessment

ABSTRACT

Among the active volcanoes worldwide, Somma-Vesuvius is one with the highest volcanic risk as the surrounding areas are highly populated. Somma-Vesuvius is quiescent since 1944, but geological and historical records reveal a frequent violent explosive activity in the last 4000 years, representing a severe risk for the ~700,000 inhabitants currently living in the area having a high probability for being impacted by pyroclastic density currents ("red zone") and more than one million people who can be potentially affected by tephra fallout. This study aims to analyze the distribution and grain-size of tephra fallout deposits from several Somma-Vesuvius eruptions of different styles, ranging from Violent Strombolian to sub-Plinian and Plinian, for characterizing the associated magmatic fragmentation through the assessment of their total grain-size distribution (TGSD). Chronologically, we focus on the Avellino (4365 BP) and Pompeii (A.D. 79) Plinian eruptions, the Pollena (A.D. 472) sub-Plinian eruption, and the 1906 and 1944 Violent Strombolian eruptions. The related TGSDs were estimated by means of the Voronoi tessellation method, which requires a suitable number of local grain-size distributions and estimation of the area of minimum tephra loading (zero-line contour). However, field-derived TGSDs can be biased towards the coarse and fine grain-size populations due to the typical paucity of available field outcrops of fallout deposits. To encompass this issue, we performed a sensitivity study on the assumption behind TGSD reconstructions and described TGSDs through analytical grain-size distributions that best fit the field TGSDs. Our main objective is a more robust estimation of the TGSDs associated with the different eruptive styles, which is crucial, together with the other eruption source parameters, for robustly predicting tephra loading and airborne ash dispersal of future eruptions at Somma-Vesuvius.

© 2019 Elsevier B.V. All rights reserved.

1. Introduction

One of the main goals of modern volcanology is a quantitative assessment of volcanic hazards (e.g. tephra loading, airborne ash dispersal) in sensitive areas like those surrounding Somma-Vesuvius, where they can heavily impact the metropolitan city of Naples (Italy) and the surrounding inhabited areas with potential severe consequences for the entire central Mediterranean zone (Folch and Sulpizio, 2010; Sulpizio et al., 2014). A robust volcanic hazard assessment requires adequate knowledge of the eruptive history of the volcano and its past behaviour (e.g. Cioni et al.,

2008; Santacroce et al., 2008). Such information is typically derived from the study of geological records (e.g. Cioni et al., 1999, 2008; Santacroce and Sbrana, 2003; Santacroce et al., 2008; Gurioli et al., 2010; Sulpizio et al., 2010a, 2010b, 2010c, 2010d, 2014), in addition to the direct observation of recent eruptive events and analysis of historical reports. Analysis of geological data allows estimation of the key eruption source parameters (ESP) of an eruption, such as total erupted mass (TEM; i.e. eruption magnitude), mass eruption rate (MER; i.e. eruption intensity) and eruptive column height. The total grain-size distribution (TGSD) of fallout deposits gives information on the intensity and behaviour of the initial magma fragmentation (Bonadonna and Houghton, 2005; Bonadonna et al., 2015; Costa et al., 2016).

In the present study, we selected four eruptions from the stratigraphic record of Somma-Vesuvius, which are representative of the

* Corresponding author.

E-mail address: matthieu.poret@gmail.com (M. Poret).

most frequent eruptive styles, to investigate the effect of different magma compositions and eruption intensity on ESPs. In particular, we considered the Avellino Plinian eruption (c.a. 3900 years BP; Sevink et al., 2011), the Pollena sub-Plinian eruption (A.D. 472; Sulpizio et al., 2005; Santacroce et al., 2008; Folch and Sulpizio, 2010), and the Violent Strombolian eruptions of 1906 (Mercalli, 1906; Arrighi et al., 2001) and 1944 (Imbò, 1949; Cubellis et al., 2013). The literature reports petrochemical and lithological features of the tephra deposits for these four eruptions (e.g. Imbò, 1949; Macedonio et al., 1988; Arrighi et al., 2001; Cioni et al., 1999, 2003a, 2003b, 2004, 2008; Sulpizio et al., 2005, 2007, 2008, 2010a, 2010b, 2010c, 2010d, 2012, 2014; Cole and Scarpati, 2010; Cubellis et al., 2013; Barsotti et al., 2015). Moreover, for comparison purposes, we took into account the Pompeii Plinian eruption (A.D. 79; Macedonio et al., 1988, 2008).

This study aims at bringing together geological data for different eruptions of different styles at Somma-Vesuvius to assess and compare the relative magma fragmentation processes, and characterize their ESPs, which is pivotal for robustly predicting tephra loading and airborne ash dispersal, and to produce risk mitigation strategies of future eruptions. TGSD is particularly required as key input parameter within tephra dispersal models (e.g. Folch, 2012). The quantification of TGSD, including ash, for each eruption can be used as an indicator for comparing magma fragmentation efficiency during the different eruptions, and its effect on the eruptive styles at Somma-Vesuvius. Assessing TGSD is also very important for characterizing the eruptive style by associating particle size distribution to the initial gas content and magma-water interaction processes (e.g. Kaminski and Jaupart, 1998; Rust and Cashman, 2011; Costa et al., 2016).

Here we assess the TGSDs of the studied eruptions (Avellino, Pollena, 1906, and 1944), ranging in eruptive style from Plinian to Violent Strombolian, by means of the Voronoi tessellation method (Bonadonna and Houghton, 2005), which integrates individual geo-referenced grain-size distributions (GSD) for each eruption. We also focus on estimating the fraction of volcanic ash finer than $10\text{ }\mu\text{m}$ (hereinafter PM₁₀) that is necessary to assess the content of airborne ash (Poret et al., 2018b) potentially affecting aviation (e.g., Folch and Sulpizio, 2010; Folch et al., 2012; Sulpizio et al., 2012). However, determination of TGSD from field data has strong limitations inherent to the sampling distance from the vent (Costa et al., 2016; Poret et al., 2018b) and the spatial and density distribution of samples along the main axis of the tephra plume (Bonadonna and Houghton, 2005; Bonadonna et al., 2015; Spanu et al., 2016). Field-derived TGSD typically tends to underestimate the fraction of either or both the coarse and fine populations (Bonadonna and Houghton, 2005; Rose and Durant, 2009; Scollo et al., 2014; Costa et al., 2016). In order to reduce the related uncertainties, we carried out a sensitivity analysis and described TGSD either as the sum of two lognormal distributions (Gaussian in Φ) or as two Weibull distributions (Costa et al., 2016, 2017; Poret et al., 2017, 2018b; Mueller et al., 2019; Pedrazzi et al., 2019) to choose the one best fitting the field-derived TGSD.

This paper presents first a brief description of the eruptive history of Somma-Vesuvius volcano, summarizing the main features of each of the studied eruptions. Then, we report the data and methodology used to estimate the relative TGSDs. Finally, we present the TGSD obtained for each eruption together with a discussion of the main findings.

2. Eruptive history of Somma-Vesuvius and selected eruptions

The Somma-Vesuvius eruptive history showed alternating effusive and explosive eruptions, sometimes associated with

destructive phases of the volcanic edifice. In particular, four Plinian eruptions associated to caldera collapses repeatedly truncated the Mt. Somma volcanic edifice, forming the present-day summit caldera (Cioni et al., 1999, 2008; Rolandi et al., 2004; Santacroce et al., 2008). These are the Pomice di Base (22.03 ± 0.18 cal ky BP; Bertagnini et al., 1998; Santacroce et al., 2008), Mercato (8.89 ± 0.09 cal ky BP; Santacroce et al., 2008; Mele et al., 2011), Avellino (3.90 ± 0.04 cal ky BP; Sevink et al., 2011; Sulpizio et al., 2010a, 2010b, 2010c, 2010d), and Pompeii (A.D. 79; Sigurdsson et al., 1985) eruptions. After the Pompeii eruption, the Vesuvius cone has progressively grown within the summit caldera reaching its present shape (Cioni et al., 2008). During its activity, several high-intensity explosive eruptions occurred at Vesuvius partly modifying the structure of the cone. These are the sub-Plinian Pollena (A.D. 472; Sulpizio et al., 2005) and A.D. 1631 (Poret et al., 2019) eruptions. The most recent cycle of Vesuvius activity between A.D. 1631 and 1944 has been characterised by recurrent summit and lateral lava effusions associated with semi-persistent and mild explosive activities, interrupted by quiescences lasting from months to a maximum of seven years (Santacroce, 1987; Cioni et al., 2008). During this period, Vesuvius produced a few Violent Strombolian eruptions, such as in 1906 and 1944. In terms of eruption magnitude (i.e. erupted volume), the Somma-Vesuvius eruptions had volumes ranging from 1 to 10 km^3 for Plinian, 0.01 to 1 km^3 for sub-Plinian, and 0.001 to 0.01 km^3 for Violent Strombolian eruptions (Cioni et al., 2008).

Hereinafter, we report a synthetic description of the main features of the eruptions considered in the present study (Avellino, Pollena, 1906, 1944), grouped in relation to the corresponding eruptive style. The Pompeii eruption is reported for comparison purposes.

2.1. Avellino and Pompeii Plinian eruptions

The Avellino eruption (3.90 ± 0.04 cal ky BP; Sevink et al., 2011) occurred in three eruptive phases: opening, magmatic Plinian, and phreatomagmatic (Sulpizio et al., 2010b, 2010c; Massaro et al., 2018). A transient short-lived eruptive column reaching 12–20 km developed during the opening phase, followed by the formation of pyroclastic density currents (PDC) from partial or total column collapse (Sulpizio et al., 2010c). The subsequent magmatic Plinian phase produced a sustained eruptive column growing from 22 to 30 km over time (Table 1). This eruptive phase ejected the main volume of tephra estimated at 1.4 km^3 , dispersed mostly north-eastwards (Cioni et al., 2003a; Sulpizio et al., 2008, 2010c). Noteworthy, tephra from the Plinian phase was found as far as Albania (Fig. 1), as recorded within the sedimentary succession of Shkodra lake at ~ 430 km from the source (Sulpizio et al., 2010a). The final phreatomagmatic phase was dominated by PDCs, producing $\sim 1\text{ km}^3$ of deposits that significantly contributed to the total erupted volume (Sulpizio et al., 2008, 2010a, 2014; Gurioli et al., 2010).

The Pompeii (A.D. 79) Plinian eruption, very famous for the destruction of the Roman towns of Pompeii and Herculaneum, has been described by numerous authors (e.g. Sigurdsson et al., 1985; Carey and Sigurdsson, 1982; Macedonio et al., 1988; Pfeiffer et al., 2005). After a brief initial phreatomagmatic vent-opening phase (Macedonio et al., 1988), the eruption was characterized by a purely magmatic Plinian phase producing a high sustained eruption column. This produced a fallout deposit subdivided into a lower layer of white phonolitic pumice (White Pumice) and an upper tephritic-phonolitic pumice (Gray Pumice) deposit (Table 1). This eruptive phase ended with the collapse of the eruptive column producing PDCs, followed by phreatomagmatic activity interpreted as the consequence of decreasing pressure in the vent and conduit. For the White Pumice and Gray Pumice layers, Sigurdsson et al. (1985)

Table 1

Main properties of the erupted products for the studied eruptions at Somma-Vesuvius.

Eruptions	Type	Composition	Vesicularity (%)	Porphyricity (%)	References
Avellino	Plinian	Phonolitic to phonolitic tephrite	80-85	16	Sulpizio et al. (2010a, 2010b, 2010c, 2010d)
Pompeii	Plinian	Phonolitic to phonolitic tephrite	50-80	4-12	Cioni et al. (1995); Gurioli et al. (2005)
Pollena 1906	Sub-Plinian	Phonolitic tephrite to tephrite phonolitic	50-60	9-12	Sulpizio et al., 2005
1944	Violent Strombolian	Phonolitic tephrite to tephrite	30-75	< 5	Bertagnini et al., 1991
	Violent Strombolian	Phonolitic tephrite to tephrite	Not available	Not available	Cioni et al., 2008

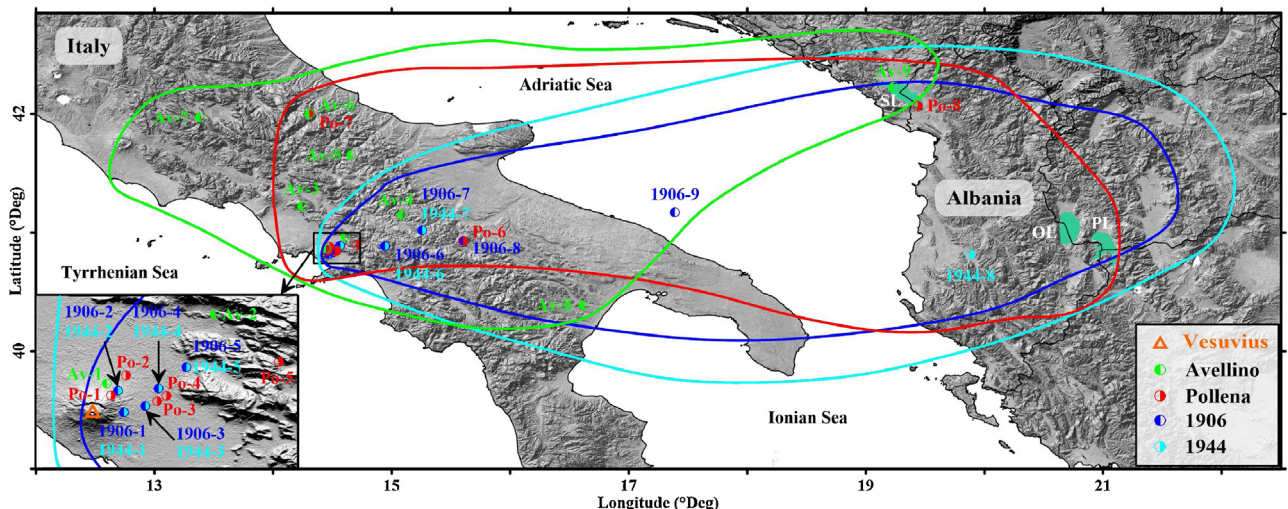


Fig. 1. Map of the main outcrops of the Avellino, Pollena, 1906, and 1944 eruptions of Somma-Vesuvius. The left-bottom inset zooms onto the proximal area. Coloured lines refer to the dispersal area of fallout deposits relevant to each eruption (modified after Sulpizio et al., 2010a, 2010b, 2010c, 2014 for Avellino; Sulpizio et al., 2005, 2010a; 2014 for Pollena; Arrighi et al., 2001; Barsotti et al., 2015 for 1906; Imbò, 1949; Cole and Scarpato, 2010; Cubellis et al., 2013 for 1944). SL, OL, and PL = Shkodra, Ohrid, and Prespa lakes (Albania and FYROM). Colours in the legend refer to the web version of this article.

estimated 2.5×10^{12} and 6.5×10^{12} kg of tephra (1 and 2.6 km^3 DRE volume), respectively. They estimated a column height increasing from 15 to 26 km during the White Pumice eruptive phase, while the column reached a maximum of 32 km (then decreased to about 27 km) during the Gray Pumice eruptive phase.

2.2. Pollena sub-Plinian eruption

Pollena (A.D. 472) is the major sub-Plinian eruption of Somma-Vesuvius, being considered by the Italian Civil Protection as one of the reference scenarios in case of renewal of explosive activity. Sulpizio et al. (2005) described the eruption as composed of three eruptive phases (opening, magmatic and phreatomagmatic), similar to the Plinian eruptions. The opening phase was characterized by a highly unstable MER, resulting in eruptive column pulses with general tephra dispersal towards north-east. The subsequent magmatic phase (Table 1) occurred through (at least) two column pulses of high eruptive intensity recorded by the deposition of pyroclastic fall beds combined with deposits from dilute to concentrate PDCs (Sulpizio et al., 2005). MER reached a peak intensity of $\sim 3.4 \times 10^7 \text{ kg/s}$ during this eruptive phase, in particular during the emplacement of the L₈ fall bed, which is the most dispersed (Sulpizio et al., 2005). The final phreatomagmatic phase was characterized by a pulsating eruptive column and emplacement of deposits from dilute to concentrate PDCs. The tephra fallout deposits relevant to the Pollena eruption dispersed north-eastwards (Fig. 1; see also Sulpizio et al., 2005), while the PDCs deposited mainly on the northern slopes of the volcano. It is worth noting that fine ash reached the Balkans, being identified in the sedimentary succession of the Shkodra lake (Sulpizio et al., 2010a) and as crypto-tephra in Ohrid lake (Sulpizio et al., 2010c). Sulpizio et al. (2005) estimated a 0.44 km^3 volume of pyroclastic fall deposits using the proximal isopachs,

increasing up to $\sim 1.38 \text{ km}^3$ with a maximum column height around 28 km by adding data from distal sites.

2.3. 1906 and 1944 Violent Strombolian eruptions

The 1906 and 1944 Violent Strombolian eruptions of Somma-Vesuvius were characterized by early effusion of lava flows followed by explosive activity (Imbò, 1949; Cioni et al., 2008). The latter typically consisted of brief but intense lava fountaining pulses associated with eruptive columns rising up to several kilometres. The activity is closed by a phreatomagmatic phase accompanied by ash emission. The 1906 and 1944 eruptions produced tephra deposits of metric thickness in the proximal areas, with distal ash deposits recognized as far as in Albania (Cubellis et al., 2013). The Violent Strombolian eruptive style is considered the most likely scenario in the case of a possible future reactivation of Somma-Vesuvius (Marzocchi et al., 2004; Neri et al., 2008).

The 1906 eruption lasted 18 days (e.g. De Lorenzo, 1906; Mercalli, 1906; Sabatini, 1906; Perret, 1924; Bertagnini et al., 1991; Scandone et al., 1993; Barsotti et al., 2015). The eruption started with an effusive phase accompanied by discontinuous ejection of incandescent material (4 days), followed by an intense lava fountaining pulse (2 days) representing the main Violent Strombolian phase (Mercalli, 1906; Barsotti et al., 2015 – Phase I). This produced an eruptive column reaching $\sim 13 \text{ km}$ above the vent (Table 1; Perret, 1924; Scandone et al., 1993) that dispersed ash to the east as far as the Adriatic Sea (Arrighi et al., 2001) and Montenegro ($\sim 400 \text{ km}$ from the vent; De Lorenzo, 1906; Barsotti et al., 2015; Fig. 1). A prolonged final phreatomagmatic phase (12 days) (Barsotti et al., 2015 – Phase II) produced abundant reddish-grey ash deposits together with millimetre-sized accretionary lapilli (De Lorenzo, 1906; Mercalli, 1906). Wind conditions, different respect to the previous phase, dispersed ash to the north-west over the city of Naples

and surroundings (Hobbs, 1906). Sabatini (1906) estimated a minimum tephra fallout volume of $\sim 0.21 \text{ km}^3$, whereas Barsotti et al. (2015) reported a TEM of $1.34 \times 10^{11} \text{ kg}$ and a bulk MER of 10^6 kg/s , with MERs of 10^6 and 10^5 kg/s for their Phase I and II, respectively. Sulpizio et al. (2012) estimated a TEM of $9.3 \times 10^{10} \text{ kg}$ and a fallout mass of $3.7 \times 10^{10} \text{ kg}$, with an average MER of $6 \times 10^4 \text{ kg/s}$ over the 18 days of eruption. Cioni et al. (2008) and references therein) reported a lower (peak) MER of $3.4 \times 10^5 \text{ kg/s}$ for the initial phase, increasing to $5.4 \times 10^6 \text{ kg/s}$ for the paroxysmal phase.

The 1944 eruption lasted 17 days, and started with the effusion of lava flows mainly along the northern slopes of the actual Vesuvius cone. The subsequent explosive phase comprised a series of 8 lava fountaining pulses over a time interval of $\sim 8 \text{ h}$ (Arrighi et al., 2001). This eruptive phase was accompanied by a steady ash column reaching heights of $\sim 5 \text{ km}$ (Scandone et al., 1993; Macedonio et al., 2008). As described by Imbò (1949), wind conditions dispersed tephra towards south-east (Fig. 1), as far as Albania where ash fallout was observed in Devoli (Cubellis et al., 2013). Cioni et al. (2008) estimated an erupted volume of $\sim 0.066 \text{ km}^3$ from the isopach map reconstructed by Pesce and Rolandi (2000). Considering a TEM of $2.2 \times 10^{12} \text{ kg}$ and a time duration of 17 days, the average MER during the eruption was of $1.5 \times 10^6 \text{ kg/s}$ (Cioni et al., 2008). Scandone et al. (1986) reported a higher MER of $4 \times 10^5 \text{ kg/s}$, whereas Macedonio et al. (2008) estimated a MER of $5 \times 10^5 \text{ kg/s}$ for modelling tephra fallout.

3. Data and methodology

3.1. Field data

The dispersal patterns of tephra deposits relevant to the studied eruptions (Fig. 1) are reconstructed mostly by using field data from the literature (e.g. Imbò, 1949; Arrighi et al., 2001; Cioni et al., 2003a; Sulpizio et al., 2005, 2007, 2010a, 2010b, 2010c, 2010d, 2012, 2014; Cole and Scarpati, 2010; Cubellis et al., 2013; Barsotti et al., 2015). The terms proximal, medial, and distal are typically used for indicating the areas affected by tephra fallout at different distances from the vent. Nonetheless, these areas can significantly vary during different eruptions because they strongly depend on eruption intensity (i.e. the column height) and atmospheric conditions (e.g. wind fields). Costa et al. (2016) proposed to delimit the areas for adequately sampling the whole tephra fallout up to $125 \mu\text{m}$ at distances from 1/10 to 10 times the eruptive column height. In this study, for the sake of simplicity, we use the term proximal to indicate distances from the source up to 30 km, medial for distances of 30–200 km, and distal for distances $> 200 \text{ km}$.

As previously mentioned, this study takes into consideration tephra samples collected for the Avellino, Pollena, 1906 and 1944 eruptions (Fig. 1; Table 2). All the details are available as Supplementary Material (Tables S1, S2, S3, and S4 respectively for the Avellino, Pollena, 1906, and 1944 eruptions). We derived field data of 9 samples regarding the Avellino eruption, mostly distributed from proximal (samples 1–2) to medial areas (samples 3–8; Sulpizio et al., 2010b), with a distal tephra sample (sample 9) found in the Shkodra lake (Sulpizio et al., 2010a). The Pollena eruption was characterized by using 8 tephra fallout samples distributed in proximal (samples 1–5), medial (samples 6–7) and distal areas (sample 8 in the Shkodra lake, Albania) derived from Sulpizio et al. (2010a). Recently, ash related to the Pollena eruption was also reported as crypto-tephra in the stratigraphic record of the Ohrid lake at the border between Albania and FYROM (Vogel et al., 2009; Sulpizio et al., 2010d), expanding significantly tephra dispersal eastwards (Fig. 1). However, we did not use this outcrop in our investigation due to the lack of grain-size analysis.

The 1906 and 1944 Violent Strombolian eruptions were characterized by means of 7 tephra samples collected at the same locations

(Table 2), representative of the proximal (samples 1–5) and medial areas (samples 6–7). Further, two other samples (samples 8 and 9) relevant to the 1906 eruption were collected in the stratigraphic record of the Monticchio lake and in a marine core offshore the city of Bari (Fig. 1), at ~ 100 and $\sim 252 \text{ km}$ from the source respectively (Fig. 1 and Table 2). A distal sample for the 1944 eruption (sample 8) was collected in Devoli, Albania, at $\sim 460 \text{ km}$ from the vent (Cubellis et al., 2013).

3.2. Estimating TGSDs

Sampling data include measurements of the tephra loading at several sites (Fig. 1 and Table 2), which are sieved for assessing the corresponding GSDs. The sieving method gives a GSD from -5 to 5 Φ (Poret et al., 2018a), where $\Phi = -\log_2 d$ and d is the particle diameter in millimetres (Krumbein, 1934). Fine ash is analysed using the Beckman Coulter Counter Multisizer™ 4 at the University of Bari, Italy, which gives GSD from 3 to 7 Φ , extending the grain-size analysis towards the tail of the grain size distribution. A normalized GSD is obtained by integrating the two partial GSDs, considering the one obtained by the sieving method as a reference. A similar procedure integrating complementary methods was successfully used in Poret et al. (2018b) for grain-size purposes. GSD includes tephra information relative to the bombs or blocks ($d \geq 64 \text{ mm}$), lapilli ($2 \text{ mm} \leq d < 64 \text{ mm}$), and ash ($d < 2 \text{ mm}$), the latter further distinguished into coarse ash ($64 \mu\text{m} \leq d < 2 \text{ mm}$) and fine ash ($d < 64 \mu\text{m}$) (e.g., Folch, 2012).

TGSD is estimated in the literature using a number of different integration methods of the individual GSDs, e.g. weighted average (Walker, 1981), sectorization of the deposit (Carey and Sigurdsson, 1982) and isomass maps (Murrow et al., 1980). In this study we use the Voronoi tessellation method by Bonadonna and Houghton (2005), considering its advantages and limitations (Bonadonna and Houghton, 2005; Bonadonna et al., 2015; Costa et al., 2016; Spanu et al., 2016; Poret et al., 2018a, 2018b). This method consists in subdividing the pyroclastic deposit into Voronoi polygons associated with georeferenced GSD for each sample. TGSD is then obtained as the weighted average of the mass distribution over the Voronoi polygons, which refers to the entire deposit. To apply this method, it is required to define the whole tephra deposit areal extent through assessment of the zero-line contour, which is the area where the deposit thickness can be assumed negligible or literally equal to zero (Bonadonna and Houghton, 2005). We assessed the zero-line contours for the studied eruptions using field data from the literature (Fig. 1). Starting from the field-based TGSDs, we also inferred TGSDs by means of general analytical distributions following the method of Costa et al. (2016, 2017). First, we considered the sum of two lognormal distributions (hereinafter bi-Gaussian in Φ -units):

$$f_{bi-Gaussian}(\Phi) = p \frac{1}{\sigma_1 \sqrt{2\pi}} e^{-\frac{(\Phi-\mu_1)^2}{2\sigma_1^2}} + (1-p) \frac{1}{\sigma_2 \sqrt{2\pi}} e^{-\frac{(\Phi-\mu_2)^2}{2\sigma_2^2}}$$

where Φ denotes particle diameter, p and $(1-p)$ are the coarse and fine sub-population weights, respectively, and μ_1 , μ_2 and σ_1 , σ_2 denote the mean and standard deviations of the two Gaussian distributions in Φ -units. Then, we used the sum of two Weibull distributions:

$$f_{bi-Weibull}(d) = q \frac{1}{n_1^{\frac{1}{n_1}}} \frac{1}{\Gamma(1 + \frac{1}{n_1})} \frac{1}{\lambda_1} \left[\frac{d}{\lambda_1} \right]^{n_1} e^{-\frac{1}{n_1} \left(\frac{d}{\lambda_1} \right)^{n_1}} + (1-q) \frac{1}{n_2^{\frac{1}{n_2}}} \frac{1}{\Gamma(1 + \frac{1}{n_2})} \frac{1}{\lambda_2} \left[\frac{d}{\lambda_2} \right]^{n_2} e^{-\frac{1}{n_2} \left(\frac{d}{\lambda_2} \right)^{n_2}}$$

Table 2

Field measurements (grain size mode and tephra loading) collected at different locations and distances from the vent for the grain-size analysis and TGSD estimation of the Avellino, Pollena, 1906 and 1944 eruptions of Somma-Vesuvius. Sample locations are also shown in Fig. 1. Details of the field data are available as Supplementary Material (Tables S1, S2, S3, and S4).

Samples	Field observations				
Avellino	Longitude	Latitude	Distance (km from source)	Mode (Φ)	Loading (kg/m ²)
Av-1	14.447	40.867	5	-3	1.80×10^2
Av-2	14.611	40.971	23	-2	1.40×10^2
Av-3	14.245	41.223	47	3	3.00×10^1
Av-4	15.091	41.151	67	1	1.20×10^2
Av-5	14.661	41.654	94	2	4.00×10^1
Av-6	14.305	42.001	131	5	3.00×10^1
Av-7	13.385	41.974	155	4	3.00×10^1
Av-8	16.619	40.388	191	5	3.00×10^1
Av-9	19.232	42.228	430	5	1.00×10^1
Pollena					
Po-1	14.454	40.849	4	-3	3.84×10^2
Po-2	14.477	40.879	8	-2	1.30×10^2
Po-3	14.524	40.839	9	-3	1.40×10^2
Po-4	40.848	14.538	10	-3	1.30×10^2
Po-5	14.708	40.899	25	-1	1.68×10^2
Po-6	15.605	40.930	100	2	3.50×10^1
Po-7	14.305	42.001	130	3	1.00×10^1
Po-8	19.440	42.070	440	6	5.00×10^1
1906					
1906-1	14.473	40.823	4	-2	5.50×10^2
1906-2	14.464	40.856	5	-2	5.50×10^2
1906-3	14.506	40.833	7	0	2.75×10^2
1906-4	14.526	40.859	10	-2	1.10×10^2
1906-5	14.567	40.891	14	-3	1.10×10^2
1906-6	14.946	40.887	44	1	1.10×10^1
1906-7	15.258	41.019	72	2	5.50×10^0
1906-8	15.605	40.931	100	3	2.20×10^0
1906-9	17.388	41.173	252	3	4.40×10^0
1944					
1944-1	14.473	40.823	4	-2	6.00×10^2
1944-2	14.464	40.856	5	-2	6.00×10^2
1944-3	14.506	40.833	7	-1	3.00×10^2
1944-4	14.526	40.859	10	-1	1.20×10^2
1944-5	14.567	40.891	14	-3	1.00×10^1
1944-6	14.946	40.887	44	1	1.20×10^1
1944-7	15.258	41.019	72	2	6.00×10^0
1944-8	19.883	40.814	460	5	1.20×10^0

where d denotes particles diameter, q and $(1-q)$ are the coarse and fine sub-population weights, respectively, and λ_1 , λ_2 and n_1 , n_2 are the scale and shape parameters of the two distributions.

4. Results and discussion

4.1. Individual grain-size distributions

The individual GSDs derived for the Avellino, Pollena, 1906 and 1944 eruptions are displayed in Figs. 2–5. Regardless of the eruption, GSDs at each location show unimodal distribution, with a clear shift of the mode from proximal to distal areas. These features are typical of tephra fallout deposits (e.g. Durant et al., 2009, 2010 for the 1980 Mt. St. Helens eruption; Watt et al., 2015 for the Chaiten eruption). The proximal samples (Fig. 1; Table 2) of each eruption have a mode ranging from -3 to 0 Φ (Table 2), with similar grain size and proportions. This indicates dominant lapilli and coarse ash up to 30 km from the source, as derived from relatively higher terminal velocities and thus deposited near the volcano (Bonadonna and Costa, 2013). In medial areas, the samples have modes ranging from 1 to 6 Φ (Table 2), covering a larger grain-size range than in the proximal area due to a larger sampling distance range (~44–191 km from the source), different eruptive column heights (from 3 to 30 km) and wind intensities (Costa et al., 2016). The modes vary from 1 to 3 Φ for the Pollena, 1906 and 1944 eruptions (Figs. 3–5, and Table 2), whereas the Avellino eruption has medial modes up to 6 Φ (Fig. 2 and Table 2). Indeed, only the Avellino eruption deposits have medial samples up to ~191 km from the

vent. Samples at similar distances from the source tend to indicate the same modes, being consistent with the main findings of Spanu et al. (2016). The distal samples have modes ranging between 5 and 6 Φ . An exception is the distal sample relevant to the 1906 eruption with a mode of 3 Φ (Fig. 4 and Table 2), but it is closer to the vent than the distal samples of the other eruptions (i.e. ~252 km from the source instead of ~430–460 km). It is worth noting that the GSDs for the studied eruptions indicate a good preservation of the tephra fallout, particularly for the fine ash (including PM₁₀) collected beyond the Apennines and Adriatic Sea up to Albania and Montenegro (Fig. 1; Sulpizio et al., 2010a, 2010d).

Given the similar evolution observed for the Plinian and sub-Plinian eruptions (see Sect. 2), we compare the GSDs of the Avellino (Plinian) and Pollena (sub-Plinian) eruptions (Figs. 2 and 3). The corresponding proximal samples show similar modes (-3 Φ at ~5 km from the source and between -2 and -1 Φ at ~25 km), proportions and sizes. The proximal GSDs of the Avellino and Pollena eruptions are also consistent with those of the Pompeii Plinian eruption reported in Macedonio et al. (1988), showing modes of -3 Φ in Pompeii (~11 km from the source) and Castellammare (~15 km), except for a sample at Maiori (~25 km) which peaks at -2 Φ . In the medial area, samples for the Avellino and Pollena eruptions located at ~100 km from the source peak at 2 Φ , and those at ~130 km have modes at 5 and 3 Φ (Table 2), respectively. According to Sulpizio et al. (2008) this feature indicates a more intense magma fragmentation with high proportion of fines produced during the Avellino eruption, especially during the magmatic Plinian phase. The distal modes for the two eruptions peak between 5 and 6 Φ for sam-

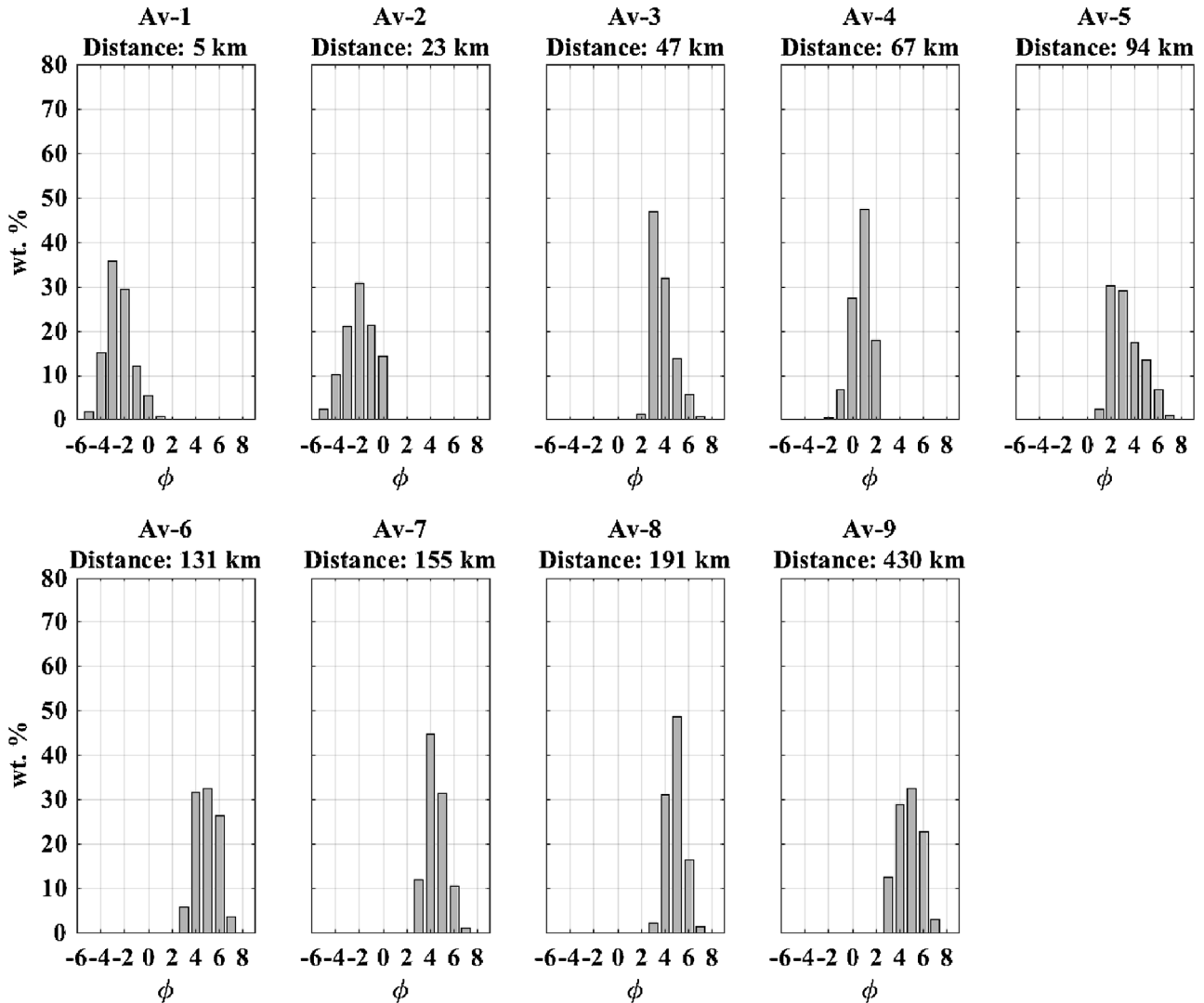


Fig. 2. Individual field-derived GSDs for the Avellino Plinian eruption at increasing distances from the vent (samples Av-1 to Av-9). Sample locations are shown in Fig. 1 and details are reported in Table 2. Details of the GSDs are available as Supplementary Material (Table S1).

ples located in the Shkodra lake, Albania (Sulpizio et al., 2010a), indicating a tephra dispersal towards north-east.

We then compare GSDs of the 1906 and 1944 Violent Strombolian eruptions (Figs. 4 and 5), noting that proximal and medial samples have a similar grain size and proportions for the same sampling sites (i.e. samples 1–7). Nonetheless, the presence of fine ash at very proximal distances from the vent (<4 km) suggests the likely occurrence of ash aggregation (Costa et al., 2010; Folch et al., 2010), presently recorded as disaggregated fine ash at the ground (Mueller et al., 2017). This interpretation was first proposed by Arrighi et al. (2001). Distal samples for the 1906 and 1944 eruptions have different modes peaking at 3 and 5 Φ , respectively (Table 2), due to different sampling distances from the vent (~252 and ~460 km, respectively). Tephra fallout during the 1906 eruption was reported in Montenegro (De Lorenzo, 1906; Barsotti et al., 2015; Fig. 1), but without the possibility of assessing the corresponding GSD due to very thin deposits.

4.2. Total grain-size distributions

First of all, it is worth noting that all the TGSD reconstructions (Fig. 6) reflect the limitations associated with the available tephra samples in terms of number and spatial distribution. Such a recon-

struction suffers from the fact that all kinds of tephra particles are considered together, without distinguishing for the different lithologies, which can have different settling behaviours. However, the reconstructed TGSDs represent the best approximations of the initial magma fragmentation for each of the studied eruptions. In this section, we describe the TGSDs reconstructed for the studied eruptions and the adopted analytical parameters (Costa et al., 2016, 2017). TGSDs are derived by using different methods, such as the Voronoi tessellation method (Bonadonna and Houghton, 2005) or the equivalent bulk grain-size distribution (Macedonio et al., 1988; Folch and Sulpizio, 2010). The results are discussed in terms of the magma fragmentation and conduit processes corresponding to different eruptive styles at Somma-Vesuvius. The dataset covers proximal, medial and distal outcrops of tephra fallout deposits relevant to the studied eruptions, even if field data are not so numerous in terms of spatial distribution. This is quite important for the TGSD estimation, as, irrespective of the eruption style, the lack of distal grain-size data can introduce a significant bias underestimating the fines (e.g. PM_{10}) and, hence, preventing proper assessment of air-borne ash, which can pose severe hazards to air traffic (Guffanti et al., 2005; Folch and Sulpizio, 2010; Sulpizio et al., 2014) and public health (Tomašek et al., 2016, 2018).

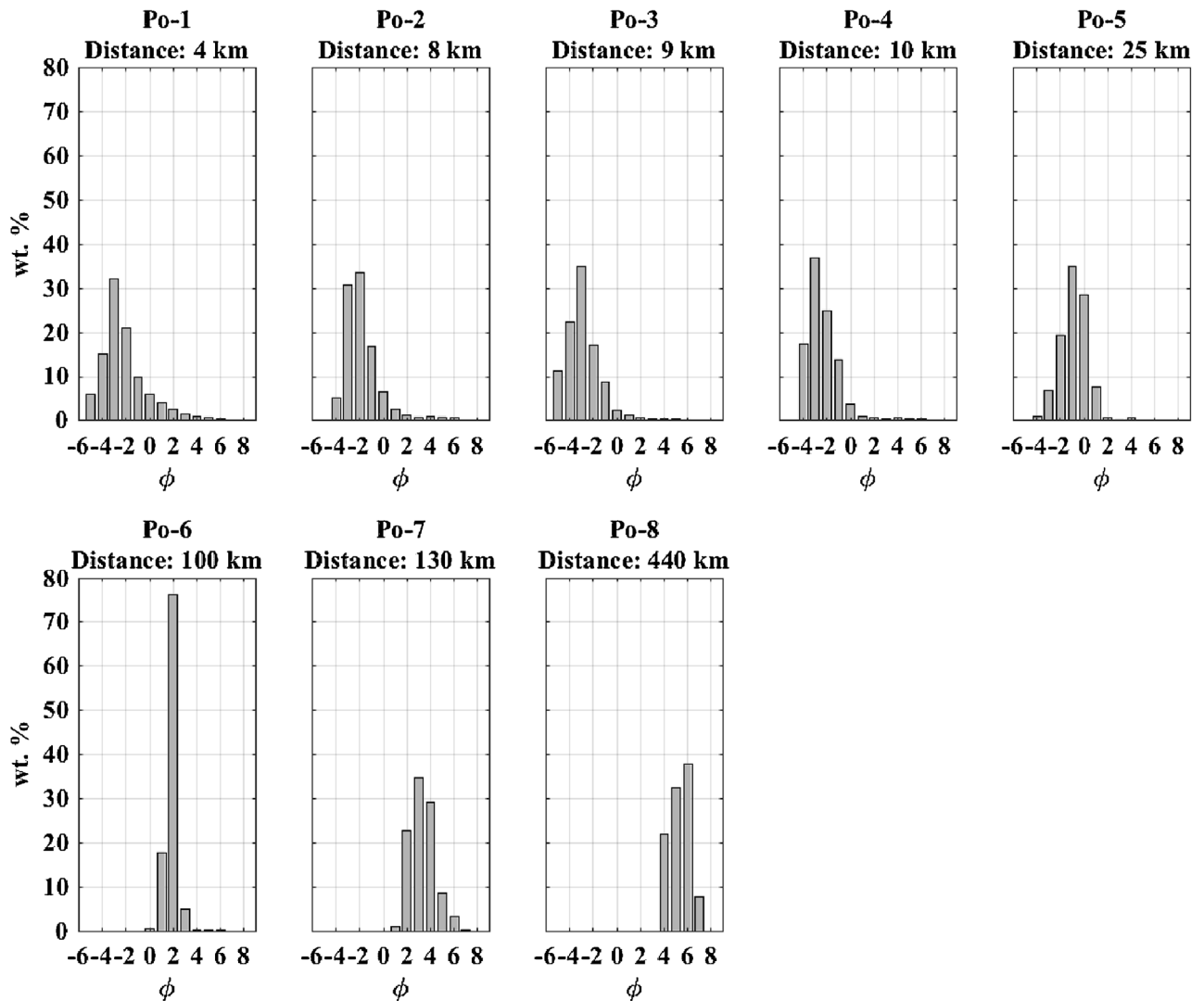


Fig. 3. Individual field-derived GSDs for the Pollena sub-Plinian eruption at increasing distances from the vent (samples Po-1 to Po-8). Sample locations are shown in Fig. 1 and details are reported in Table 2. Details of the GSDs are available as Supplementary Material (Table S2).

TGSDs are first estimated from field data (Fig. 6). All the reconstructed TGSDs show an overall bimodality pattern for coarse and fine sub-populations, except for that related to the 1944 eruption. The Avellino eruption TGSD peaks at 1 and 4 Φ , the Pollena eruption TGSD at -1 and 6 Φ , and the 1906 eruption TGSD at 0 and 3 Φ . For comparison, the TGSD of the Pompeii Plinian eruption peaks at 1 and 5 Φ (Macedonio et al., 2008), in agreement with our TGSDs derived for the Avellino Plinian eruption and the Pollena sub-Plinian eruption. Also, the Pollena eruption TGSD estimated by Folch and Sulpizio (2010) assuming an equivalent bulk grain-size distribution derived from massive PDC deposits peaks at 1 and 4–5 Φ , consistently with the TGSDs for the Avellino and Pompeii eruptions. Differently, the 1944 eruption TGSD shows a unique mode at -2 Φ , which is more similar to lower intensity eruptions involving magmas at lower viscosity (Costa et al., 2016). Considering the different eruptive styles of the studied eruptions, the resulting field-based TGSDs indicate modes shifting towards the fines when the eruption intensity increases (from Violent Strombolian to Plinian), in agreement with the analysis performed in Costa et al. (2016).

As a second step, we obtained TGSDs for the studied eruptions by means of the Voronoi tessellation method. This particularly requires availability of a suitable number of samples well dispersed

along the main tephra dispersal axis (i.e. proximal, medial, and distal areas), and a careful definition of the tephra edge defined as the zero-line contour (Bonadonna and Houghton, 2005; Bonadonna et al., 2015). The dispersal areas of the eruptions are reconstructed on the basis of the tephra extents available in the literature (see Sect. 2). As for the uncertainty related to the definition of the zero-line contour, Volentik et al. (2010) raised uncertainties on the standard deviation of the modes and fine ash component of the TGSDs. Nonetheless, these uncertainties are much higher when tephra deposits are not sampled correctly, i.e. not including sites up to distal areas (Bonadonna et al., 2015).

During an eruption producing tephra fallout, very fine ash (e.g. PM_{10}) is released into the atmosphere where it can remain for days to weeks dispersing towards distal areas (Rose and Durant, 2009). This fine material, if escaped to aggregation processes, is very difficult to be sampled due to its very long residence time in the atmosphere. It follows that PM_{10} are typically under-estimated, biasing the field-derived TGSDs in the fines and preventing a correct assessment of the airborne ash mass and its relative concentration (Poret et al., 2018a, 2018b). On this, we showed that Plinian eruptions (e.g. Avellino and Pompeii) may produce around 80 wt. % of ash with a PM_{10} content of few percent (Table 4). This can have a strong impact on air traffic safety producing extended areas

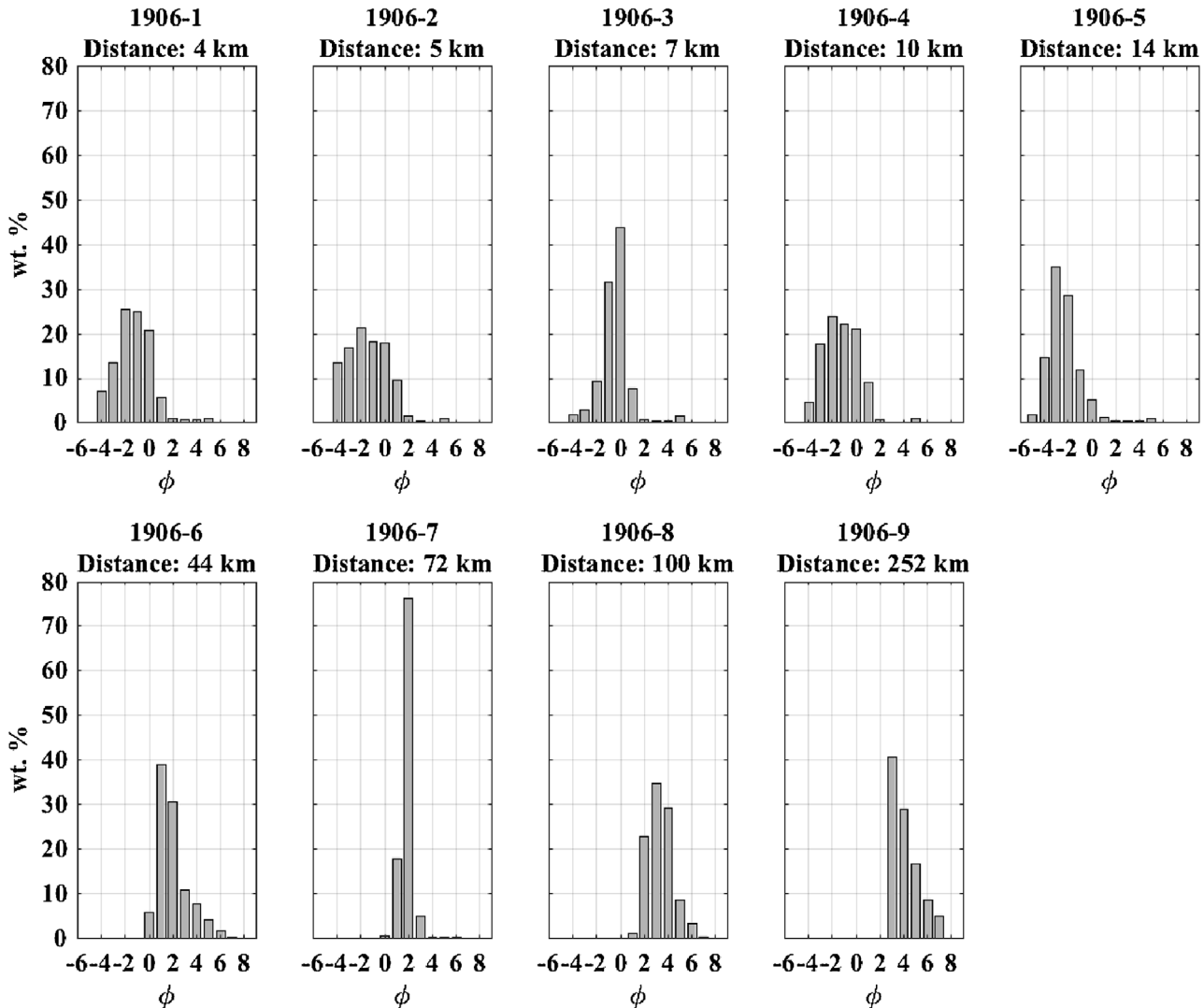


Fig. 4. Individual field-derived GSDs for the 1906 Violent Strombolian eruption at increasing distances from the vent (samples 1906-1 to 1906-9). Sample locations are shown in Fig. 1 and details are reported in Table 2. Details of the GSDs are available as Supplementary Material (Table S3).

with ash concentration above the threshold of 4 mg/m^3 (Gouhier et al., 2019 and references therein), thus delimiting the no-fly zones. Gouhier et al. (2019) recently demonstrated that the more intense eruptions (i.e. Plinian) are the least efficient in transporting airborne PM₁₀, due to early en masse fallout. This explains why we regularly observe ash in proximal and medial areas, but it also suggests that the measured PM₁₀ fraction is a minimum amount to be considered. A few studies have attempted to assess this fraction at Etna (Sicily, Italy) by integrating field and remote sensing data (i.e. satellite and/or X-band radar retrievals; Poret et al., 2018a, 2018b). Although the PM₁₀ fraction may be negligible compared to the bulk tephra, it is critical for operational tephra dispersal models (like those used by the Volcanic Ash Advisory Centers).

Considering the absence of remote sensing data for the studied eruptions, we need other methods for trying to better capture the fine and coarse tails of field-based TGSDs. The TGSD are thus described by means of bi-Gaussian and bi-Weibull distributions, which allow extrapolations. The distributions best fitting the field-based TGSDs are estimated by assuming two main tephra populations (coarse and fine) as described in Costa et al. (2016, 2017). Costa et al. (2016) showed that bimodality of TGSDs is a common feature for several tephra fallout deposits. This is also the case of the present study that shows asymmetric and clear bimodal sig-

nature for the TGSDs of most of the studied eruptions (Fig. 6). The 1944 eruption is an exception because its TGSD, although asymmetric, has a more unimodal pattern. The general bimodality (or in some cases multimodality; Fig. 6) derives from superimposition of the grain-size distribution of various components (juvenile, lithics and loose crystals; Mele et al., 2019), along with a different degree of vesicularity of coarse and fine-grained juveniles (Table 1). Other factors, like secondary fragmentation (Jones and Russel, 2017) or phreatomagmatism, may play a role. For better classifying whether TGSDs are bimodal or unimodal, Costa et al. (2016) used a bimodality index (*BI*) for bi-Gaussian distributions as follows:

$$BI = \sqrt{2} \frac{|\mu_1 - \mu_2|}{\sqrt{\sigma_1^2 + \sigma_2^2}} \sqrt{p(1-p)}$$

where μ_i and σ_i are the modes and standard deviations of the Gaussian distributions (Sect. 3.2). The best fitting parameters for the studied eruptions are reported in Table 3, together with the associated *BI* values.

The obtained *BI* values tend to indicate bimodal distributions for all the TGSDs, except for those of the Pollena eruption estimated from Folch and Sulpizio (2010) and the 1944 eruption. The latter have a more unimodal distribution, although the corresponding

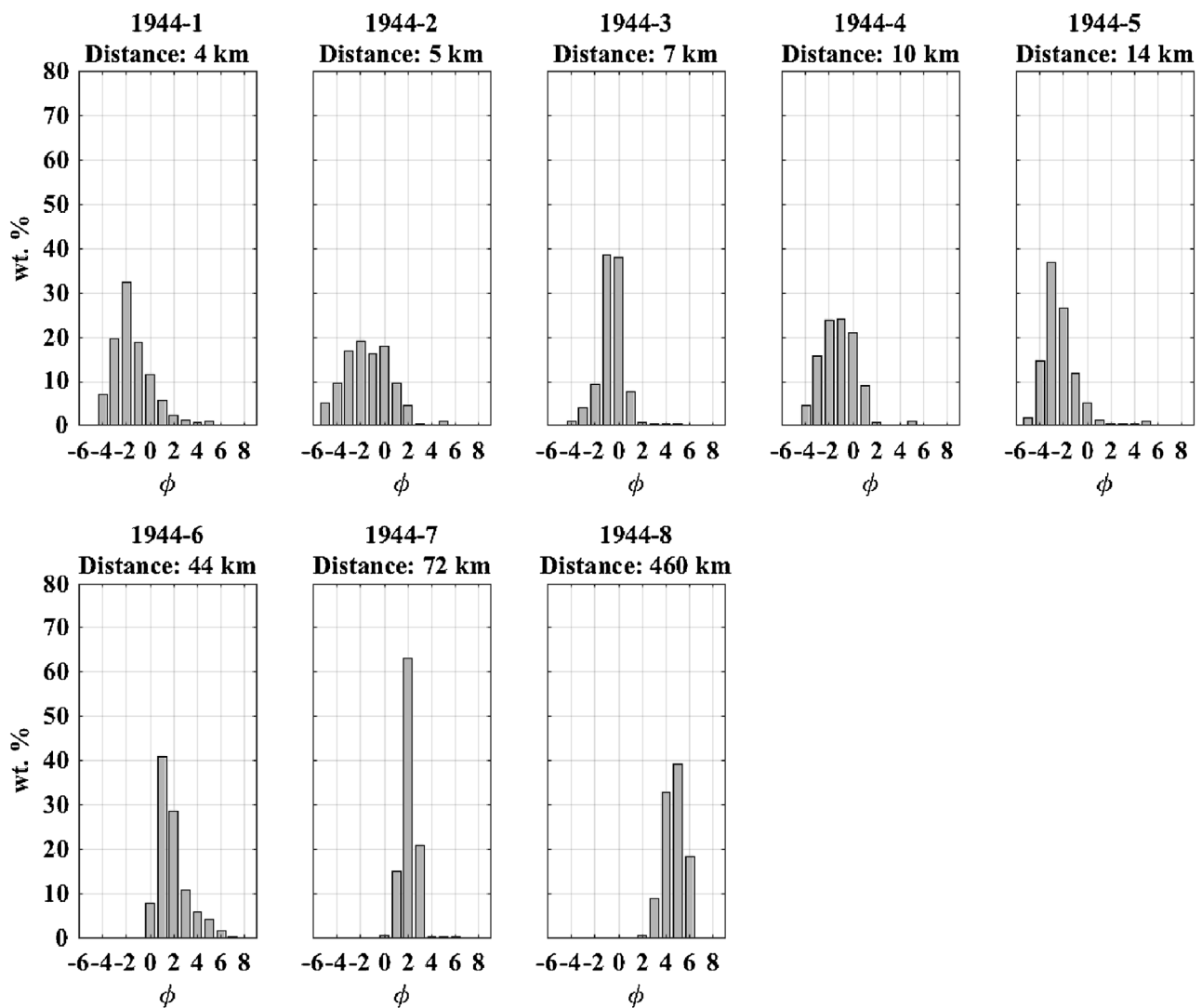


Fig. 5. Individual field-derived GSDs for the 1944 Violent Strombolian eruption at increasing distances from the vent (samples 1944-1 to 1944-8). Sample locations are shown in Fig. 1 and details are reported in Table 2. Details of the GSDs are available as Supplementary Material (Table S4).

Table 3

Parameters of the bi-Gaussian and bi-Weibull distributions best fitting the field-based TGSDs for the Avellino, Pompeii, Pollena, 1906 and 1944 eruptions: p and $(1-p)$ are, respectively, the coarse and fine sub-population weights; μ_1 , μ_2 and σ_1 , σ_2 are the mean and standard deviations of the two Gaussian distributions in Φ -units; q and $(1-q)$ are, respectively, the coarse and fine sub-population weights; λ_1 , λ_2 and n_1 , n_2 are the scale and shape parameters of the two distributions. Bimodality for the Gaussian distributions is assumed for $BI > 1.1$ (Costa et al., 2016). * Data related to the TGSD from Macedonio et al. (2008). ** Data related to the TGSD from Folch and Sulpizio (2010).

bi-Gaussian	Avellino	Pompeii *	Pollena	Pollena **	1906	1944
$\mu_1 (\Phi)$	0.29 ± 0.07	0.14 ± 0.26	-0.78 ± 0.46	0.28 ± 0.16	-1.52 ± 0.17	-2.74 ± 0.10
$\sigma_1 (\Phi)$	1.16 ± 0.06	2.48 ± 0.21	2.60 ± 0.38	2.86 ± 0.13	1.64 ± 0.14	1.34 ± 0.08
$\mu_2 (\Phi)$	4.12 ± 0.23	5.32 ± 0.25	4.99 ± 0.17	4.87 ± 0.16	3.08 ± 0.11	0.08 ± 0.24
$\sigma_2 (\Phi)$	1.10 ± 0.19	1.04 ± 0.20	0.92 ± 0.14	1.22 ± 0.13	1.10 ± 0.09	2.53 ± 0.20
p	0.77 ± 0.02	0.78 ± 0.03	0.63 ± 0.04	0.79 ± 0.02	0.53 ± 0.03	0.48 ± 0.03
BI	1.41	1.13	1.43	0.85	1.65	0.70
bi-Weibull						
λ_1 (in mm)	0.41 ± 0.04	0.43 ± 0.07	1.28 ± 0.31	0.54 ± 0.08	1.27 ± 0.12	4.82 ± 0.28
n_1	0.65 ± 0.03	0.38 ± 0.01	0.42 ± 0.03	0.37 ± 0.01	0.40 ± 0.01	0.95 ± 0.05
λ_2 (in mm)	0.03 ± 0.01	0.02 ± 0.01	0.02 ± 0.01	0.02 ± 0.01	0.07 ± 0.01	0.84 ± 0.07
n_2	1.16 ± 0.40	0.88 ± 0.15	0.98 ± 0.12	0.75 ± 0.07	1.16 ± 0.06	0.30 ± 0.01
q	0.86 ± 0.04	0.74 ± 0.04	0.56 ± 0.05	0.68 ± 0.04	0.60 ± 0.02	0.32 ± 0.02

TGSDs are made of coarse and fine sub-populations that are close enough to show a unimodal-like shape (Fig. 6). TGSD is needed as an input parameter for tephra dispersal models typically in the form of discrete size bins. The TGSD bins obtained from field data for the studied eruptions are reported in the Appendix (Tables A1–A6),

together with those related to the corresponding best-fitting bi-Gaussian and bi-Weibull distributions.

We discuss below the main insights on magma fragmentation processes for the studied eruptions derived from the TGSDs reconstructed by putting together field data and the relative analytical

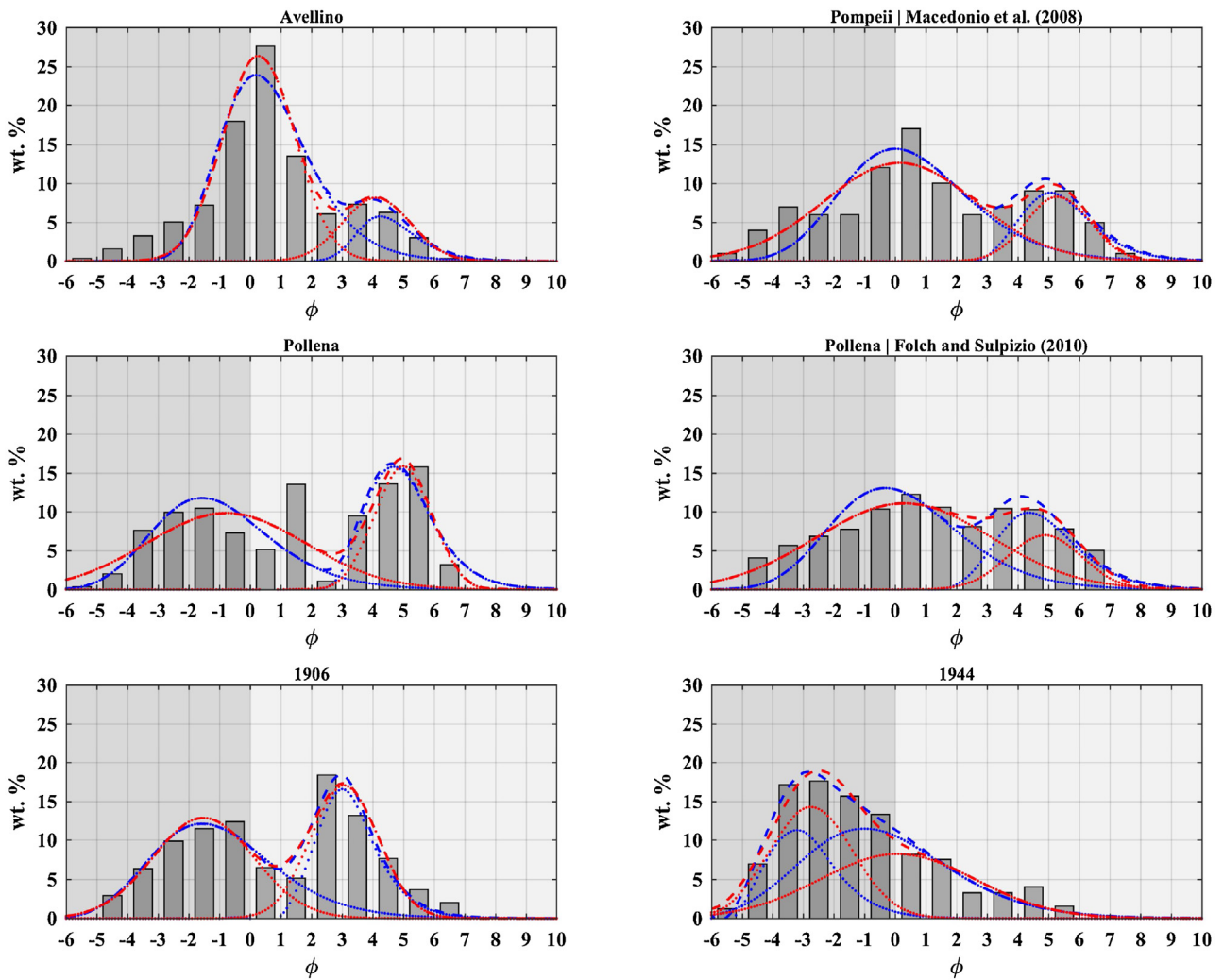


Fig. 6. Field-based TGSDs (bars) for the Avellino, Pollena, 1906 and 1944 eruptions. Another field-based TGSD for the Pompeii eruption is derived from massive PDC deposits by [Folch and Sulpizio \(2010\)](#). A field-based TGSD for the Pompeii eruption from [Macedonio et al. \(2008\)](#) is used for comparison with that of the Avellino eruption. Red and blue lines show the bi-Gaussian and bi-Weibull distributions, respectively, best fitting the field-based TGSDs. The dotted lines refer to the sub-populations of the relative distributions. Further details on the distributions are given in Sect. 3.2, and [Tables 3 and 4](#). Grey colours are consistent with [Tables 4](#) and A (see Appendix).

distributions (i.e. bi-Gaussian and bi-Weibull). For the sake of simplicity, [Table 4](#) reports the mass fractions associated with each grain-size class (i.e. bombs/blocks, lapilli, coarse and fine ash).

We first compare the results for the Avellino Plinian eruption and Pollena sub-Plinian eruption because they had a similar evolution even if they are classified with a different eruptive style. The TGSD for the Avellino eruption have modes at 0–1 Φ and at 4 Φ for the coarse and fine sub-populations, respectively, whereas the Pollena eruption TGSD have modes at -2 to -1 Φ and at 5–6 Φ ([Fig. 6; Table A1](#)). The relative sub-populations amounts indicate for the Pollena eruption a relatively coarser tephra deposit than for the Avellino eruption, with a greater production of lapilli (~30 vs. ~18 wt.%; [Tables A1 and A2](#)). The Avellino eruption instead produced substantially more ash than the Pollena eruption (~80 vs. ~60 wt.%; [Tables A1, A3 and 1](#)). Going further in detail, the Avellino eruption produced more coarse ash than the Pollena eruption (~70 vs. ~35 wt.%), whereas the Pollena eruption released more fine ash (~8 vs. ~30 wt.%) and PM₁₀ (~4 and ~1 wt.%; [Tables A1 and A3](#)). This seems to indicate a more efficient magma fragmentation for the Pollena eruption, although it showed very unstable eruptive conditions. It is worth noting that the magmatic phase of the Avellino eruption was followed by a final phreatomagmatic phase characterized by an energy drop affecting magma fragmentation

([Sulpizio et al., 2008, 2010b](#)), which could have determined a lower fraction of fine ash compared to the Pollena eruption. [Sulpizio et al. \(2005\)](#) explained this in terms of varying magma fragmentation efficiency but they also mentioned the possible occurrence of an extensive magma-water interaction during the final phase able to control eruption dynamics and increase magma fragmentation in the course of the Pollena eruption.

We then compare the field-derived TGSDs of the Avellino and Pompeii eruptions, both of Plinian eruptive style. For the Pompeii eruption we used the TGSD estimated by [Macedonio et al. \(1988, 2008\)](#) from an individual GSD relative to an outcrop of massive PDC deposits derived from the eruptive column collapse (see [Fig. 2b](#) therein). Regarding the fine ash content, [Macedonio et al. \(1988\)](#) considered all the bin fractions corresponding to $\Phi \geq 5$ all together as fine residual at $\Phi = 5$. This makes a comparison with our TGSD subdivided into different fine fractions not very significant. The coarse mode of the Pompeii eruption peaking at 1 Φ is instead fully consistent with our results for the Avellino eruption. The Pompeii eruption yields a substantially higher content in lapilli (~37 vs. ~18 wt.%; [Table 4](#)), and, thus, a lower content in ash (~63 vs. ~82 wt.%) compared to the Avellino eruption. Moreover, the Pompeii eruption TGSD shows a slightly higher content in fine ash (~14 vs. ~10 wt.%). In a subsequent paper, [Macedonio et al. \(2008\)](#)

Table 4

Fractions of the different grain size classes used in this study: bombs ($\Phi \leq -6$), lapilli ($-5 \leq \Phi \leq -1$), and ash ($0 \leq \Phi$). Ash is further subdivided in coarse ($4 \leq \Phi \leq 0$) and fine ($\Phi \leq 5$) as described in Folch (2012). The PM_{10} fraction corresponds to ash fragments with diameter below $10 \mu\text{m}$ as in Poret et al. (2018b). The fractions are expressed in weight percentage (wt. %) and refer to the field-derived TGSDs, and the bi-Gaussian and bi-Weibull distributions reconstructed for the Avellino, Pollena, 1906 and 1944 eruptions. Grey shades are consistent with Tables A (see Appendix) and Fig. 6. * Data extracted from Macedonio et al. (2008). ** Data extracted from Folch and Sulpizio (2010).

	Class	Field-TGSD	bi-Gaussian	bi-Weibull
Avellino	Bombs	0.00	0.00	0.00
	Lapilli	17.62	18.70	19.71
	Ash	82.38	81.29	80.28
	Coarse ash	72.65	73.14	72.15
	Fine ash	9.73	8.15	8.13
	PM_{10}	0.35	0.29	0.81
Pompeii*	Total	100	100	100
	Bombs	0.00	0.59	0.00
	Lapilli	23.98	30.29	24.80
	Ash	78.28	69.12	75.20
	Coarse ash	52.11	48.77	52.17
	Fine ash	24.17	20.35	23.03
Pollena	PM_{10}	6.05	2.95	5.21
	Total	100	100	100
	Bombs	0.00	1.31	0.12
	Lapilli	30.58	32.53	36.10
	Ash	69.44	66.17	63.79
	Coarse ash	36.71	38.48	35.12
Pollena **	Fine ash	32.73	27.69	28.67
	PM_{10}	3.26	1.71	4.58
	Total	100	100	100
	Bombs	0.00	0.99	0.01
	Lapilli	24.53	29.34	26.89
	Ash	75.12	69.67	73.09
1906	Coarse ash	51.84	50.80	53.12
	Fine ash	23.28	18.87	19.97
	PM_{10}	5.10	2.93	4.08
	Total	100	100	100
	Bombs	0.00	0.31	0.19
	Lapilli	30.78	38.73	38.10
1944	Ash	69.22	60.95	61.70
	Coarse ash	55.78	56.72	56.48
	Fine ash	13.44	4.23	5.22
	PM_{10}	2.07	0.03	0.40
	Total	100	100	100
	Bombs	0.00	1.21	0.42
	Lapilli	58.73	65.92	65.77
	Ash	41.28	32.86	33.80
	Coarse ash	35.66	30.83	31.54
	Fine ash	5.62	2.03	2.26
	PM_{10}	0.02	0.27	0.52
	Total	100	100	100

reported a bulk TGSD for the Pompeii eruption as representative of the granulometry of Plinian/Sub-Plinian eruptions at Somma-Vesuvius. We also made the attempt of reconstructing a TGSD for the Pompeii eruption through a bi-Gaussian and bi-Weibull distribution best-fitting field data. Both the TGSDs are displayed in Fig. 6 for a comparison with the Avellino eruption TGSD. It shows a mode at 0–1 Φ for the coarse population and at 5 Φ for the fine population (Tables A1, A2). The relative TGSDs indicate comparable values for lapilli and ash (Table 4), suggesting acceptable results although the paucity of field data implies large uncertainties on the TGSD assessment. In detail, the TGSD for the Pompeii eruption from Macedonio et al. (2008) shows comparable values with respect to the other TGSDs, with ~24 and ~76 wt. % of lapilli and ash, respectively. Regarding the ash, there is an amount of ~52, 24 and ~6 wt. % of coarse, fine ash, and PM₁₀, respectively. It follows that all the TGSDs estimated for Plinian eruptions (i.e. Avellino and Pompeii) are in agreement, with a dominancy of ash (between 60 and 80 wt. %) during magma fragmentation. This is consistent with Rose and Durant (2009) who discussed how silicic eruptions can contain substantial fractions of ash.

With a similar approach, we compare our TGSD obtained for the Pollena eruption with the one derived by Folch and Sulpizio (2010) (see Fig. 6) on the basis of an individual GSD relative to an outcrop of massive PDC deposits representative of eruptive column collapse. We derived a TGSD by best-fitting their field-based TGSD with bi-Gaussian and bi-Weibull distributions. The obtained TGSD peaks at 0–1 Φ and 4 Φ for the coarse and fine populations, respectively. This is slightly different from our TGSD for the Pollena eruption (see Tables A3, A4), which can be attributed to a different method. Particularly, we obtained a TGSD composed of two grain size populations more marked than in the TGSD derived from Folch and Sulpizio (2010). Our TGSD has a coarser proximal deposit with ~31 wt. % of lapilli instead of ~25 wt. % estimated by Folch and Sulpizio (2010). Regarding the class fractions (Table 4), Folch and Sulpizio (2010) obtained ~75 wt. % of ash, whereas our TGSD indicates ~69 wt. %. Furthermore, they suggest ~52, 23 and ~5 wt. % of coarse ash, fine ash and PM₁₀, whereas we have ~37, 33 and ~3 wt. %, respectively. These results all go in the direction of saying that magma fragmentation during the Pollena eruption produced ~30 wt. % of lapilli and ~70 wt. % of ash, with ~45 wt. % of coarse ash, ~30 wt. % of fine ash, and ~4 wt. % of PM₁₀. These results are very similar to those obtained for the Plinian eruptions, thus reinforcing the similarity observed between Plinian and sub-Plinian eruptions.

Further discussion regards the Violent Strombolian 1906 and 1944 eruptions. The TGSD reconstructed in the present study for the 1906 eruption has a first mode at -2 to 0 Φ for the coarse sub-population and a second mode at 3 Φ for the fine sub-population (Table 4; Fig. 6). The 1944 eruption yields a significantly different TGSD showing a fairly unimodal pattern with a main mode between -3 and -2 Φ . Indeed, a second mode characterizing the fine sub-population peaks at -1 and 0 Φ (respectively for the bi-Weibull and bi-Gaussian distributions) but it is not clearly visible as partially overlapped to the coarse sub-population (see Fig. 6). The discrepancy between the TGSDs related to the 1906 and 1944 eruptions can be interpreted as the result of different magma fragmentation processes. Particularly, the higher amount of fines produced during the 1906 eruption could be explained in terms of higher intensity of the eruption and influence of magma-water interaction during the major final phreatomagmatic phase (Costa et al., 2016). In fact, these results, together with the features of the Pollena TGSD, support the importance of magma-water interaction controlling magma fragmentation (Sulpizio et al., 2010b). Comparing the class fractions, the TGSD of the 1906 eruption has a substantially lower content in lapilli than that of the 1944 eruption (~31 vs. ~59 wt. %; Table 4), but a higher content in ash (~69 vs. ~41 wt. %; Table 4).

A large quantity of lapilli during the 1944 eruption is also reported by Arrighi et al. (2001), together with a substantial production of ash aggregates up to centimetre size. Regarding the fines, the 1906 eruption is shown to have produced more coarse (~56 vs. ~36 wt. %) and fine ash (~13 vs. ~6 wt. %; Table 4), and also PM₁₀ fraction (~2 vs. < 1 wt. %), than the 1944 eruption.

In summary, the results of TGSDs analysis for the studied eruptions allow identification of distinctive grain-size features for the different eruptive styles at Somma-Vesuvius, although the paucity of available field data prevents to assume the reconstructed TGSDs as fully representative of the initial magma fragmentation conditions. Results indicate that an increased intensity of the eruptions (passing from Violent Strombolian to Plinian) is associated to a shift of the main modes of the TGSDs towards the fines (Fig. 6 and Tables A). In particular, we show that the Plinian eruptions (e.g. Avellino and Pompeii) produce the greatest amount of ash with up to ~82 wt. % (Table 4). This was also reported by Costa et al. (2016), who defined parameters to estimate TGSD in terms of bulk magma viscosity and column height, and observed the mode shifting towards the fines when increasing magma viscosity and eruption intensity values. Further, we consider the abundance of fines in some other eruptions as the result of a more efficient magma fragmentation at the source. On this, the Pollena sub-Plinian eruption (ash = ~70 wt. %, PM₁₀ = ~4 wt. %) and the 1906 Violent Strombolian eruption (ash = ~69 wt. %, PM₁₀ = ~2 wt. %) are associated to an exceptional magma fragmentation efficiency in contrast with the Avellino, Pompeii, and 1944 eruptions, likely in relation with a substantial influence of magma-water interaction processes.

5. Conclusions

This study presents grain-size analyses related to a number of tephra samples associated with some eruptions of Somma-Vesuvius, assumed as reference for different eruptive styles of the volcano (from Violent Strombolian to Plinian), with the aim of assessing the impact of magma fragmentation on the eruptive styles. Chronologically, we focus on the Avellino Plinian eruption (3900 yr BP), the Pollena sub-Plinian eruption (A.D. 472), and the 1906 and 1944 Violent Strombolian eruptions. Previous estimations of the Pompeii Plinian (A.D. 79) and Pollena eruptions were used for comparison purposes. Field-based individual grain-size distributions were integrated using the Voronoi tessellation method for assessing the total grain size distribution (TGSD) relative to each eruption. We also defined TGSDs by means of analytical bi-Gaussian and bi-Weibull distributions best-fitting the field-derived ones. Results indicate that an increased eruption intensity, passing from Violent Strombolian to Plinian eruptions, and an efficient magma-water interaction are associated to a shift of the TGSD modes towards the fines, as the evidence of an enhanced magma fragmentation at the source. This is largely consistent with the literature, reinforcing previous findings and reopening the interest of studying magma fragmentation from field data, but not limited to them. The present study could be a good example of the importance of studying tephra distribution produced by volcanic eruptions worldwide from Violent Strombolian to Sub-Plinian and Plinian eruptive styles. In particular, our main findings could be used to numerically reconstruct past eruptions or forecast similar eruptive scenarios at Somma-Vesuvius, and to assess tephra loading and/or airborne ash mass from the source towards distal regions.

Declaration of Competing Interest

None.

Acknowledgements

MP has been partially supported by the FP 7 Marie Curie Actions Framework (FP7-PEOPLE-2013-ITN): VERTIGO: volcanic ash: field, experimental, and numerical investigations of processes during its lifecycles (grant agreement number 607905). A.C. acknowledges the European project EUROVOLC (grant agreement number 731070) and the Ministero dell'Istruzione, dell'Università e della

ricerca (MIUR, Roma, Italy) Ash-RESILIENCE project (grant agreement number 805 FOE 2015). We are very grateful to U. Kueppers and the Editor for their careful reviews that helped to improve the clarity of the manuscript. S. Baranello is warmly acknowledged for revising the English.

Appendix A.

Table A1

Field-derived TGSD and the corresponding bi-Gaussian and bi-Weibull distributions for the Avellino Plinian eruption. TGSDs are expressed in weight percentage (wt. %) of the different class-fractions, and displayed in Fig. 6. The related grain-size class fractions are reported in Table 4. Grey shades conform to Fig. 6 and Table 4.

Diameter (Φ)	Field TGSD	bi-Gaussian	bi-Weibull
-6	0.00	0.00	0.00
-5	0.35	0.00	0.00
-4	1.61	0.03	0.00
-3	3.31	0.49	0.26
-2	5.09	3.83	4.07
-1	7.26	14.35	15.38
0	18.00	25.72	23.69
1	27.66	22.17	20.60
2	13.53	10.31	12.46
3	6.13	6.65	7.42
4	7.33	8.29	7.98
5	6.31	5.95	5.28
6	3.07	1.91	2.04
7	0.35	0.27	0.60
8	0.00	0.02	0.16
9	0.00	0.00	0.04
10	0.00	0.00	0.01

Table A2

Field-derived TGSD for the Pompeii Plinian eruption from Macedonio et al. (2008), together with the corresponding bi-Gaussian and bi-Weibull distributions reconstructed in the present study. TGSDs are expressed in weight percentage (wt. %) of the different class-fractions, and displayed in Fig. 6. The related grain-size class fractions are reported in Table 4. Grey shades conform to Fig. 6 and Table 4.

Diameter (Φ)	Field TGSD	bi-Gaussian	bi-Weibull
-6	0.00	0.59	0.00
-5	1.00	1.47	0.10
-4	3.98	3.13	0.80
-3	7.00	5.65	3.32
-2	6.00	8.69	7.97
-1	6.01	11.35	12.61
0	12.03	12.59	14.43
1	17.03	11.88	12.88
2	10.04	9.58	9.49
3	6.01	7.19	6.71
4	7.00	7.53	8.66
5	9.06	9.87	10.54
6	9.07	7.53	7.28
7	5.03	2.53	3.39
8	1.02	0.38	1.27
9	0.00	0.04	0.42
10	0.00	0.00	0.13

Table A3

Field-derived TGSD and the corresponding bi-Gaussian and bi-Weibull distributions for the Pollena sub-Plinian eruption. TGSDs are expressed in weight percentage (wt. %) of the different class fractions, and displayed in Fig. 6. The related grain-size class fractions are reported in Table 4. Grey shades conform to Fig. 6 and Table 4.

Diameter (Φ)	Field TGSD	bi-Gaussian	bi-Weibull
-6	0.00	1.31	0.12
-5	0.38	2.63	1.04
-4	2.08	4.56	3.95
-3	7.67	6.81	8.38
-2	9.97	8.77	11.45
-1	10.48	9.76	11.28
0	7.32	9.36	8.70
1	5.18	7.74	5.59
2	13.57	5.61	3.15
3	1.15	4.96	4.03
4	9.49	10.81	13.65
5	13.65	16.86	15.55
6	15.82	9.12	8.54
7	3.26	1.59	3.22
8	0.00	0.11	1.00
9	0.00	0.01	0.28
10	0.00	0.00	0.08

Table A4

Field-derived TGSD for the Pollena sub-Plinian eruption from Folch and Sulpizio (2010), together with the corresponding bi-Gaussian and bi-Weibull distributions reconstructed in the present study. TGSDs are expressed in weight percentage (wt. %) of the different class-fractions, and displayed in Fig. 6. The related grain-size class fractions are reported in Table 4. Grey shades conform to Fig. 6 and Table 4.

Diameter (Φ)	Field TGSD	bi-Gaussian	bi-Weibull
-6	0.00	0.99	0.01
-5	0.00	2.00	0.20
-4	4.14	3.60	1.27
-3	5.70	5.72	4.28
-2	6.92	8.03	8.79
-1	7.76	9.99	12.35
0	10.36	11.00	12.92
1	12.31	10.76	10.78
2	10.59	9.66	8.17
3	8.14	9.18	9.28
4	10.44	10.20	11.97
5	10.33	9.86	10.09
6	7.86	6.08	5.80
7	5.10	2.22	2.60
8	0.00	0.54	1.00
9	0.00	0.13	0.36
10	0.00	0.04	0.12

Table A5

Field-derived TGSD and the corresponding bi-Gaussian and bi-Weibull distributions for the 1906 Violent Strombolian eruption. TGSDs are expressed in weight percentage (wt. %) of the different class-fractions, and displayed in Fig. 6. The related grain-size class fractions are reported in Table 4. Grey shades conform to Fig. 6 and Table 4.

Diameter (Φ)	Field TGSD	bi-Gaussian	bi-Weibull
-6	0.00	0.31	0.19
-5	0.00	1.35	1.30
-4	2.90	4.11	4.42
-3	6.41	8.59	8.85
-2	9.91	12.38	11.84
-1	11.56	12.30	11.69
0	12.44	8.72	9.15
1	6.53	6.78	6.32
2	5.17	11.81	12.01
3	18.41	17.34	18.40
4	13.23	12.07	10.60
5	7.67	3.70	3.74
6	3.70	0.50	1.08
7	2.07	0.03	0.29
8	0.00	0.00	0.08
9	0.00	0.00	0.02
10	0.00	0.00	0.01

Table A6

Field-derived TGSD and the corresponding bi-Gaussian and bi-Weibull distributions for the 1944 Violent Strombolian eruption. TGSDs are expressed in weight percentage (wt. %) of the different class-fractions, and displayed in Fig. 6. The related grain-size class fractions are reported in Table 4. Grey shades conform to Fig. 6 and Table 4.

Diameter (Φ)	Field TGSD	bi-Gaussian	bi-Weibull
-6	0.00	1.21	0.42
-5	1.20	4.57	3.14
-4	6.96	11.48	12.88
-3	17.20	18.00	18.68
-2	17.66	18.18	16.98
-1	15.71	13.69	14.09
0	13.36	10.00	11.37
1	8.21	7.98	8.54
2	7.54	6.18	5.85
3	3.26	4.21	3.66
4	3.29	2.46	2.12
5	4.03	1.23	1.15
6	1.57	0.53	0.59
7	0.02	0.19	0.29
8	0.00	0.06	0.14
9	0.00	0.02	0.06
10	0.00	0.00	0.03

Appendix B. Supplementary data

Supplementary material related to this article can be found, in the online version, at doi:<https://doi.org/10.1016/j.jvolgeores.2019.106683>.

References

- Arrighi, S., Principe, C., Rosi, M., 2001. Violent strombolian and sub-Plinian eruptions at Vesuvius during post-1631 activity. Bull. Volcanol. 63, 126–150, <http://dx.doi.org/10.1007/s00445-0100130>.
- Barsotti, S., Neri, A., Bertagnini, A., Cioni, R., Mulas, M., Mundula, F., 2015. Dynamics and tephra dispersal of Violent Strombolian eruptions at Vesuvius: insights from field data, wind reconstruction and numerical simulation of the 1906 event. Bull. Volcanol. 77, 58, <http://dx.doi.org/10.1007/s00445-015-0939-6>.
- Bertagnini, A., Landi, P., Santacroce, R., Sbrana, A., 1991. The 1906 eruption of Vesuvius: from magmatic to phreatomagmatic activity through the flashing of a shallow depth hydrothermal system. Bull. Volcanol. 53, 517–532.
- Bertagnini, A., Landi, P., Rosi, M., Vigliarotto, A., 1998. The Pomici di Base Plinian eruption of Somma-Vesuvius. J. Volcanol. Geotherm. Res. 83 (3), 219–239.
- Bonadonna, C., Houghton, B.F., 2005. Total grain-size distribution and volume of tephra-fall deposits. Bull. Volcanol. 67, 441–456, <http://dx.doi.org/10.1007/s00445-004-0386-2>.
- Bonadonna, C., Costa, A., 2013. Plume height, volume, and classification of explosive volcanic eruptions based on the Weibull function. Bull. Volcanol. 75, 742, <http://dx.doi.org/10.1007/s00445-013-0742-1>.
- Bonadonna, C., Biass, S., Costa, A., 2015. Physical characterization of explosive volcanic eruptions based on tephra deposits: propagation of uncertainties and sensitivity analysis. J. Volcanol. Geotherm. Res. 296, 80–100, <http://dx.doi.org/10.1016/j.jvolgeores.2015.03.009>.
- Carey, S.N., Sigurdsson, H., 1982. Influence of particle aggregation on deposition of distal tephra from the May 18, 1980, eruption of Mount St-Helens volcano. J. Geophys. Res. 87 (B8), 7061–7072, <http://dx.doi.org/10.1029/JB087iB08p07061>.
- Cioni, R., Civetta, L., Marianelli, P., Metrich, N., Santacroce, R., Sbrana, A., 1995. Compositional layering and syn-eruptive mixing of a periodically refilled shallow magma chamber: the AD 79 plinian eruption of Vesuvius. J. Petrol. 36, 739–776.
- Cioni, R., Santacroce, R., Sbrana, A., 1999. Pyroclastic deposits as a guide for reconstructing the multi-stage evolution of the Somma-Vesuvius caldera. Bull. Volcanol. 60, 207–222.
- Cioni, R., Longo, A., Macedonio, G., Santacroce, R., Sbrana, A., Sulpizio, R., Andronico, D., 2003a. Assessing pyroclastic fall hazard through field data and numerical simulations: example from Vesuvius. J. Geophys. Res. 108 (B2), 2063, <http://dx.doi.org/10.1029/2001JB000642>.
- Cioni, R., Sulpizio, R., Garruccio, N., 2003b. Variability of the eruption dynamics during a Subplinian event: the Greenish Pumice eruption of Somma-Vesuvius (Italy). J. Volcanol. Geotherm. Res. 124 (1–2), 89–114, [http://dx.doi.org/10.1016/S0377-0273\(03\)00070-2](http://dx.doi.org/10.1016/S0377-0273(03)00070-2).

- Cioni, R., Gurioli, L., Lanza, R., Zanella, E., 2004. Temperature of the A.D. 79 pyroclastic density current deposits (Vesuvius, Italy). *J. Geophys. Res.* 109, B02207, <http://dx.doi.org/10.1029/2002JB002251>.
- Cioni, R., Bertagnini, A., Santacroce, R., Andronico, D., 2008. Explosive activity and eruption scenarios at Somma-Vesuvius (Italy): towards a new classification scheme. *J. Volcanol. Geotherm. Res.* 178, 331–346, <http://dx.doi.org/10.1016/j.jvolgeores.2008.04.024>.
- Cole, P.D., Scarpatti, C., 2010. The 1944 eruption of Vesuvius, Italy: combining contemporary accounts and field studies for a new volcanological reconstruction. *Geol. Mag.* 147 (3), 391–415, <http://dx.doi.org/10.1017/S0016756809990495>.
- Costa, A., Folch, A., Macedonio, G., 2010. A model for wet aggregation of ash particles in volcanic plumes and clouds: 1. Theoretical formulation. *J. Geophys. Res.* 115, B09201, <http://dx.doi.org/10.1029/2009JB007175>.
- Costa, A., Pioli, L., Bonadonna, C., 2016. Assessing tephra total grain-size distribution: insights from field data analysis. *Earth Planet. Sci. Lett.* 443, 90–107, <http://dx.doi.org/10.1016/j.epsl.2016.02.040>.
- Costa, A., Pioli, L., Bonadonna, C., 2017. Corrigendum to “Assessing tephra total grain-size distribution: Insights from field data analysis”. [*Earth and Planetary Sci. Lett.* 443, 90–107, 2016]. *Earth and Planetary Sci. Lett.*, <http://dx.doi.org/10.1016/j.epsl.2017.03.003>.
- Cubellis, E., Marturano, A., Pappalardo, L., 2013. *Le ceneri distali dell’eruzione del Vesuvio del marzo 1944 raccolte a Devoli (Albania)*. Quaderni di geofisica 113, in italiano.
- De Lorenzo, G., 1906. *The eruption of Vesuvius in April 1906*. Q. J. Geol. Soc. 62, 476–483.
- Durant, A.J., Rose, W.I., Sarna-Wojcicki, A.M., Carey, S., Volentik, A.C.M., 2009. Hydrometeor-enhanced tephra sedimentation: constraints from the 18 May 1980 eruption of Mount St. Helens. *J. Geophys. Res.* 114, <http://dx.doi.org/10.1029/2008JB005756>, B03204.
- Durant, A.J., Bonadonna, C., Horwell, C.J., 2010. Atmospheric and environmental impacts of volcanic particulates. *Elements* 6, 235–240, <http://dx.doi.org/10.2113/gselements.6.4.235>.
- Folch, A., Sulpizio, R., 2010. Evaluating long-range volcanic ash hazard using supercomputing facilities: application to Somma-Vesuvius (Italy), and consequences for civil aviation over the Central Mediterranean Area. *Bull. Volcanol.* 72, 1039–1059, <http://dx.doi.org/10.1007/s00445-010-0386-3>.
- Folch, A., Costa, A., Durant, A., Macedonio, G., 2010. A model for wet aggregation of ash particles in volcanic plumes and clouds: 2. Model application. *J. Geophys. Res.* 115, B09202, <http://dx.doi.org/10.1029/2009JB007176>.
- Folch, A., 2012. A review of tephra transport and dispersal models: evolution, current status, and future perspectives. *J. Volcanol. Geotherm. Res.* 235–236, 96–115, <http://dx.doi.org/10.1016/j.volgeores.2012.05.020>.
- Folch, A., Costa, A., Basart, S., 2012. Validation of the FALL3D ash dispersion model using observations of the 2010 Eyjafjallajökull volcanic ash clouds. *Atmos. Env.* 48, 165–183, <http://dx.doi.org/10.1016/j.atmosenv.2011.06.072>.
- Gouhier, M., Eychenne, J., Azaoui, N., Guillain, A., Deslandes, M., Poret, M., Costa, A., Husson, P., 2019. Low efficiency of large volcanic eruptions in transporting very fine ash into the atmosphere. *Nature Sci. Rep.* 9, 1449, <http://dx.doi.org/10.1038/s41598-019-38595-7>.
- Guffanti, M., Ewert, J.W., Gallina, G.M., Bluth, G.J.S., Swanson, G.L., 2005. Volcanic-ash hazard to aviation during the 2003–2004 eruption activity of Anatahan volcano Commonwealth of the Northern Mariana Islands. *J. Volcanol. Geotherm. Res.* 146, 241–255, <http://dx.doi.org/10.1016/j.volgeores.2004.12.011>.
- Gurioli, L., Houghton, B.F., Cashman, K.V., Cioni, R., 2005. Complex changes in eruption dynamic during the 79 AD eruption of Vesuvius. *Bull. Volcanol.* 67, 144–159.
- Gurioli, L., Sulpizio, R., Cioni, R., Sbrana, A., Santacroce, R., Luperini, W., Andronico, D., 2010. Pyroclastic flow hazard assessment at Somma-Vesuvius based on the geological record. *Bull. Volcanol.* 72, 1021–1038, <http://dx.doi.org/10.1007/s00445-010-0379-2>.
- Hobbs, W.H., 1906. *The grand eruption of Vesuvius in 1906*. J. Geol. 14–17, 636–655.
- Imbò, G., 1949. *L’attività eruttiva e relative osservazioni nel corso dell’intervallo inter-eruttivo 1906–1944 ed in particolare del parossismo del Marzo 1944*. Annali Osservatorio Vesuviano, pp. 185–380, V serie, volume unico, in italiano.
- Jones, T.J., Russel, J.K., 2017. Ash production by attrition in volcanic conduits and plumes. *Nature Sci. Rep.* 7, 5538, <http://dx.doi.org/10.1038/s41598-017-05450-6>.
- Kaminski, E., Jaupart, C., 1998. The size distribution of pyroclasts and the fragmentation sequence in explosive volcanic eruptions. *J. Geophys. Res.* 103 (B12), 29759–29779, <http://dx.doi.org/10.1029/98JB02795>.
- Krumbein, W.C., 1934. Size frequency distribution of sediments. *J. Sediment. Res.* 4 (2), 65–77, <http://dx.doi.org/10.1306/D4268EB9-2B26-11D7-8648000102C1865D>.
- Macedonio, G., Pareschi, M.T., Santacroce, R., 1988. A numerical Simulation of Plinian Fall Phase of 79 A.D. Eruption of Vesuvius. *J. Geophys. Res.* 93 (B12), 14817–14827, <http://dx.doi.org/10.1029/B093B12p14817>.
- Macedonio, G., Costa, A., Folch, A., 2008. Ash fallout scenarios at Vesuvius: numerical simulations and implications for hazard assessment. *J. Volcanol. Geotherm. Res.* 178 (3), 366–377, <http://dx.doi.org/10.1016/j.jvolgeores.2008.08.014>.
- Marzocchi, W., Sandri, L., Gasperini, P., Newhall, C., Boschi, E., 2004. Quantifying probabilities of volcanic events: the example of volcanic hazard at Mount Vesuvius. *J. Geophys. Res.* 109, B11201, <http://dx.doi.org/10.1029/2004JB003155>.
- Massaro, S., Costa, A., Sulpizio, R., 2018. Evolution of the magma feeding system during a Plinian eruption: the case of Pomice di Avellino eruption of Somma-Vesuvius, Italy. *Earth Planetary Sci. Lett.* 482, 545–555, <http://dx.doi.org/10.1016/j.epsl.2017.11.030>.
- Mele, D., Sulpizio, R., Dellino, P., La Volpe, L., 2011. Stratigraphy and eruptive dynamics of a pulsating Plinian eruption of Somma-Vesuvius: the Pomice di Mercato (8900 years B.P.). *Bull. Volcanol.* 73, 257–278, <http://dx.doi.org/10.1007/s00445-010-0407-2>.
- Mele, D., Costa, A., Dellino, P., Sulpizio, R., Dioguardi, F., Isaia, R., and Macedonio, G. Total grain size distribution of components of fallout deposits and implications for magma fragmentation mechanisms: examples from Campi Flegrei caldera (Italy). *Bull. Volcanol.* Submitted.
- Mueller, S.B., Kueppers, U., Ametsbichler, J., Cimarelli, C., Merrison, J.P., Poret, M., Wadsworth, F.B., Dingwell, D.B., 2017. Stability of volcanic ash aggregates and break-up processes. *Nature – Sci. Rep.* 7, 7440, <http://dx.doi.org/10.1038/s41598-017-07927-w>.
- Mueller, S.B., Houghton, B.F., Swanson, D.A., Fagents, S.A., Klawonn, M., Poret, M., 2019. *Total grain-size distribution of a Hawaiian tephra deposit: case study of the 1959 Kilauea Iki eruption Hawai’i*. *Bull. Volcanol.* xxx, xx–xx, doi:xxxxxxxx.
- Murrow, P.J., Rose, W.I., Self, S., 1980. Determination of the total grain size distribution in a Vulcanian eruption column, and its implications to stratospheric aerosol perturbation. *Geophys. Res. Lett.* 7 (11), 893–896, <http://dx.doi.org/10.1029/GL007i011p00893>.
- Neri, A., Aspinall, W.P., Cioni, R., Bertagnini, A., Baxter, P.J., Zuccaro, G., Andronico, D., Barotti, S., Cole, P.D., Esposito Ongaro, T., Hincks, T.K., Macedonio, G., Papale, P., Rosi, M., Santacroce, R., Woo, C., 2008. Developing an Event Tree for pyroclastic hazard and risk assessment at Vesuvius. *J. Volcanol. Geotherm. Res.* 178, 397–415, <http://dx.doi.org/10.1016/j.jvolgeores.2008.05.014>.
- Pedrazzi, D., Suñe-Puchol, I., Aguirre-Díaz, G., Costa, A., Smith, V.C., Poret, M., Dávila-Harris, P., Miggins, D.P., Hernández, W., Gutierrez, E., 2019. The Ilopango Tierra Blanca Joven (TBj) eruption, El Salvador: Volcano-stratigraphy and physical characterization of the major Holocene event of Central America. *J. Volcanol. Geotherm. Res.* 377, 81–102, <http://dx.doi.org/10.1016/j.jvolgeores.2019.03.006>.
- Perret, F.A., 1924. *The Vesuvius Eruption of 1906. Study of a Volcanic Cycle*. Carnegie Inst Washington Pub 339, pp 151.
- Pesce, A., Rolandi, G., 2000. *Vesuvio 1944. L’ultima eruzione*. Edizioni Magma, Napoli, p. 216.
- Poret, M., Costa, A., Folch, A., Martì, A., 2017. Modelling tephra dispersal and ash aggregation: The 26th April 1979 eruption, La Soufrière St. Vincent. *J. Volcanol. Geotherm. Res.* 347, 207–220, <http://dx.doi.org/10.1016/j.jvolgeores.2017.09.012>.
- Poret, M., Corradini, S., Merucci, L., Costa, A., Andronico, D., Vulpiani, G., Montopoli, M., Freret-Lorgeril, V., 2018a. Reconstructing volcanic plume evolution integrating satellite and ground-based data: application to the 23 November 2013 Etna eruption. *Atmos. Chem. Phys.* 18 (7), 4695–4714, <http://dx.doi.org/10.5194/acp-18-4695-2018>.
- Poret, M., Costa, A., Andronico, D., Scollo, S., Gouhier, M., Cristaldi, A., 2018b. Modelling eruption source parameters by integrating field, ground-based and satellite-based measurements: the case of the 23 February 2013 Etna paroxysm. *J. Geophys. Res. Solid Earth* 123, <http://dx.doi.org/10.1029/2017JB015163>.
- Poret, M., Finizola, A., Ricci, T., Ricciardi, G.P., Linde, N., Mauri, G., Barde-Cabusson, S., Guichet, X., Baron, L., Shakas, A., Gouhier, M., Levieux, G., Morin, J., Rouleau, E., Sortino, F., Vasallo, R., Di Vito, M.A., Orsi, G., 2019. The buried boundary of Vesuvius 1631 caldera revealed by present-day diffuse degassing. *J. Volcanol. Geotherm. Res.* 375, 43–56, <http://dx.doi.org/10.1016/j.jvolgeores.2019.01.029>.
- Rolandì, G., Bellucci, F., Cortini, M., 2004. A new model for the formation of the Somma Caldera. *Mineral. Petro.* 80, 27–44, <http://dx.doi.org/10.1007/s00710-003-0018-0>.
- Rose, W.I., Durant, A.J., 2009. Fine ash content of explosive eruptions. *J. Volcanol. Geotherm. Res.* 186 (1–2), 32–39, <http://dx.doi.org/10.1016/j.jvolgeores.2009.01.010>.
- Rust, A.C., Cashman, K.V., 2011. Permeability controls on expansion and size distributions of pyroclasts. *J. Geophys. Res.* 116, B11202, <http://dx.doi.org/10.1029/2011JB008494>.
- Sabatini, V., 1906. *L’eruzione vesuviana dell’Aprile 1906*. Boll. Del R. 3, 169–229, Comitato geologico d’Italia, in Italian.
- Santacroce, R., 1987. *Somma-Vesuvius. Quaderni. Ric. Sci.* 114, 230, Cons. Naz. delle Ric. Rome.
- Santacroce, R., Sbrana, A., 2003. *Geological map of Vesuvius at the scale 1:15,000*. SELCA editore, Firenze.
- Santacroce, R., Cioni, R., Marianelli, P., Sbrana, A., Sulpizio, R., Zanchetta, G., Donahue, D.J., Joron, J.L., 2008. Age and whole rock-glass compositions of proximal pyroclastics from the major explosive eruptions of Somma-Vesuvius: a review as a tool for distal tephrostratigraphy. *J. Volcanol. Geotherm. Res.* 177, 1–18, <http://dx.doi.org/10.1016/j.jvolgeores.2008.06.009>.
- Scandone, R., Iannone, F., Mastrolorenzo, G., 1986. *Stima dei parametri dinamici dell’eruzione del 1944 del Vesuvio*. Boll. GNV 2, 487–512.
- Scandone, R., Giacomelli, L., Gasparini, P., 1993. *Mount Vesuvius: 2000 yrs of volcanic observations*. J. Volcanol. Geotherm. Res. 58, 263–271.
- Scollo, S., Prestifilippo, M., Pecora, E., Corradini, S., Merucci, L., Spata, G., Coltellini, M., 2014. Eruption column height estimation of the 2011–2013 Etna lava fountains. *Annals Geophys.* 57 (2), S0214, <http://dx.doi.org/10.4401/ag-6396>.
- Sevink, J., Van Bergen, M.J., Van der Plicht, J., Feiken, H., Anastasia, C., Huizinga, A., 2011. *Robust date for the Bronze Age Avellino eruption (Somma-Vesuvius): 3945 ± 10 cal BP (1995 ± 10 cal BC)*. *Quat. Sci. Rev.* 30, 1035–1046.
- Sigurdsson, H., Carey, S., Cornell, W., Pescatore, T., 1985. *The eruption of Vesuvius A.D. 79*. *Nat. Geo. Res.* 1 (3), 332–387.
- Spanu, A., De Vitturi, M.M., Barsotti, S., 2016. Reconstructing eruptive source parameters from tephra deposit: a numerical study of medium-sized explosive

- eruptions at Etna volcano. Bull. Volcanol. 78 (9), 59, <http://dx.doi.org/10.1007/s00445-016-1051-2>.
- Sulpizio, R., Mele, D., Dellino, P., La Volpe, L., 2005. A complex, Subplinian-type eruption from low-viscosity, phonolitic to tephriphonolitic magma: the AD 472 (Pollena) eruption of Somma-Vesuvius, Italy. Bull. Volcanol. 67, 743–767, <http://dx.doi.org/10.1007/s00445-005-0414-x>.
- Sulpizio, R., Mele, D., Dellino, P., La Volpe, L., 2007. Deposits and physical properties of pyroclastic density currents during complex Subplinian eruptions: the AD 472 (Pollena) eruption of Somma-Vesuvius, Italy. Sedimentology 54 (3), 607–635, <http://dx.doi.org/10.1111/j.1365-3091.2006.00852.x>.
- Sulpizio, R., Caron, B., Giaccio, B., Paterne, M., Siani, G., Zanchetta, G., Santacroce, R., 2008. The Dispersal of Ash during Explosive Eruptions From Central Volcanoes and Calderas: an Underestimated Hazard for the Central Mediterranean Area. IOP Publishing, <http://dx.doi.org/10.1088/1755-1307/3/1/012031>, Collapse Calderas Workshop, Series 3.
- Sulpizio, R., Van Welden, A., Caron, B., Zanchetta, G., 2010a. The Holocene tephrostratigraphic record of Lake Shkodra (Albania and Montenegro). J. Quat. Sci. 25 (5), 633–650, <http://dx.doi.org/10.1002/jqs.1334>.
- Sulpizio, R., Cioni, R., Di Vito, M.A., Mele, D., Bonasia, R., Dellino, P., 2010b. The Pomice di Avellino eruption of Somma-Vesuvius (3.9 ka BP) part I: stratigraphy, compositional variability and eruptive dynamics. Bull. Volcanol. 72, 539–558, <http://dx.doi.org/10.1007/s00445-009-0339-x>.
- Sulpizio, R., Bonasia, R., Dellino, P., Mele, D., Di Vito, M.A., La Volpe, L., 2010c. The Pomice di Avellino eruption of Somma-Vesuvius (3.9 ka BP) part II: sedimentology and physical volcanology of pyroclastic density current deposits. Bull. Volcanol. 72, 559–577, <http://dx.doi.org/10.1007/s00445-009-0340-4>.
- Sulpizio, R., Zanchetta, G., D'Orazio, M., Vogel, H., Wagner, B., 2010d. Tephrostratigraphy and tephrochronology of lakes Ohrid and Prespa, Balkans. Biogeosciences 7, 3273–3288, <http://dx.doi.org/10.5194/bg-7-3273-2010>.
- Sulpizio, R., Folch, A., Costa, A., Scaini, C., Dellino, P., 2012. Hazard assessment of far-range volcanic ash dispersal from a violent Strombolian eruption at Somma-Vesuvius volcano, Naples, Italy: implications on civil aviation. Bull. Volcanol. 74, 2205–2218, <http://dx.doi.org/10.1007/s00445-012-0656-3>.
- Sulpizio, R., Zanchetta, G., Caron, B., Dellino, P., Mele, D., Giaccio, B., Insinga, D., Paterne, M., Siani, G., Costa, A., Macedonio, G., Santacroce, R., 2014. Volcanic ash hazard in the Central Mediterranean assessed from geological data. Bull. Volcanol. 76, 866, <http://dx.doi.org/10.1007/s00445-014-0866-y>.
- Tomašek, I., Horwell, C.J., Damby, D.E., Barošová, H., Geers, C., Petri-Fink, A., Rothen-Rutishauser, B., Clift, M.J.D., 2016. Combined exposure of diesel exhaust particles and respirable Soufrière Hills volcanic ash causes a (pro-)inflammatory response in an *in vitro* multicellular epithelial tissue barrier model. Part. Fibre Toxicol. 13 (1), 67, <http://dx.doi.org/10.1186/s12989-016-0178-9>.
- Tomašek, I., Horwell, C.J., Bisig, C., Damby, D.E., Comte, P., Czerwinski, J., Petri-Fink, A., Clift, M.J.D., Drasler, B., Rothen-Rutishauser, B., 2018. Respiratory hazard assessment of combined exposure to complete gasoline exhaust and respirable volcanic ash in a multicellular human lung model at the air-liquid interface. Env. Pollution 238, 977–987, <http://dx.doi.org/10.1016/j.envpol.2018.01.115>.
- Vogel, H., Zanchetta, G., Sulpizio, R., Wagner, B., Nowaczyk, N., 2009. A tephrostratigraphic record for the last glacial-interglacial cycle from Lake Ohrid, Albania and Macedonia. J. Quat. Sci. 25 (3), 320–338, <http://dx.doi.org/10.1002/jqs.1311>.
- Volentik, A.C.M., Bonadonna, C., Connor, C.B., Connor, L.J., Rosi, M., 2010. Modeling tephra dispersal in absence of wind: Insights from the climactic phase of the 2450 BP Plinian eruption of Pululagua volcano (Ecuador). J. Volcanol. Geotherm. Res. 193 (1–2), 117–136.
- Walker, G.P.L., 1981. The Waimihia and Hatepe plinian deposits from the rhyolitic Taupo Volcanic Centre. New Zealand J. Geol. Geophys. 24 (3), 305–324.
- Watt, S.F.L., Gilbert, J.S., Folch, A., Phillips, J.C., 2015. An example of enhanced tephra deposition driven by topographic induced atmospheric turbulence. Bull. Volcanol. 77, 35, <http://dx.doi.org/10.1007/s00445-015-0927-x>.